Laponite® Nanoparticle Doped Polyelectrolyte Hydrogels

Jiyuan Wu

Department of Chemical Engineering
McGill University, Montreal
April, 2022

A thesis submitted to McGill University in partial fulfillment of the requirements of the degree of

Master of Science

Abstract

Introducing nano-materials into polymeric hydrogels often enhances mechanical strength and toughness. With the advantages of hydrogels, such as biocompatibility, biodegradability and porosity, the resulting hydrogel nanocomposites are often termed 'smart' drug carriers, in the case of this research, pH-responsive hydrogels, demonstrating efficient transport and targeted, controlled release. However, due to nano-composite opacity and high-nano-particle loading, the widely available light-scattering diagnostics for particle size and ζ-potential are not readily applied to nano-composite hydrogels. In the other hand, electroacoustic characterization, can provide micro-structural insights by registering the so-called electrokinetic sonic amplitude (ESA). ESA has recently been applied to uncharged nanoparticle-doped hydrogels, and charged hydrogels without nanoparticles. This thesis examines, for the first time, the electroacoustic response of a model polyelectrolyte hydrogel with charged nanoparticle inclusions: Laponite® XLG-doped acrylamide-*co*-acrylic acid hydrogels. The acrylic-acid monomer fraction and Laponite® concentration were systematically varied in the ranges 0–1 and 0–1 wt%, respectively, reporting the ESA, conductivity, and linear viscoelasticity. Comparing these data to benchmark literature on acrylamide-*co*-acrylic acid based hydrogels (without nanoparticles), Laponite® was found to increase the ESA and conductivity, but decrease the stiffness. Quantitative interpretations were undertaken using theoretical models for the ESA and conductivity. The decrease in stiffness with Laponite®-doping contrasts with many studies on Laponite®-doped poly(acrylamide)- and poly(acrylic acid)-based hydrogels. This

seems to reflect a high degree of acrylic acid neutralization, which promotes electrostatic repulsion between Laponite® and the polymer network, thus transforming Laponite® to a much more passive nano-particulate filler at neutral pH. This observation may have beneficial technological implications, e.g., promoting NP release. Further insights were gained by comparing polymeric hydrogels with their monomer-solution counterparts, enabling the effects of polymerization and cross-linking to be examined in more detail.

Abrégé

L'introduction de nanomatériaux dans des hydrogels polymères améliore souvent la résistance mécanique et la ténacité. Avec les avantages des hydrogels, tels que la biocompatibilité, la biodégradabilité et la porosité, les nanocomposites d'hydrogel qui en résultent sont souvent appelés vecteurs médicaux intelligents, démontrant un transport efficace et une libération contrôlée ciblée. Cependant, en raison de l'opacité nano-composite et de la charge élevée en nano-particules (NP), les diagnostics par diffusion de la lumière largement disponibles pour la taille des particules et le potentiel ζ ne sont pas facilement appliqués aux hydrogels nano-composites. En revanche, la caractérisation électroacoustique peut fournir des informations sur les micro-structures en enregistrant l'amplitude sonique électrocinétique (ASE). L'ASE a récemment été appliquée à des hydrogels non-chargés dopés aux nanoparticules non chargés et à des hydrogels chargés sans nanoparticules. Cette thèse examine, pour la première fois, la réponse électroacoustique d'un modéle d'hydrogel polyélectrolyte modèle avec des inclusions de nanoparticules chargées: des hydrogels d'acrylamide-*co*-acide acrylique dopés Laponite® XLG. La fraction de monomère d'acide acrylique et la concentration de Laponite® ont été systématiquement variées dans les gammes 0–1 et 0–1 wt %, respectivement, rapportant l'ASE, la conductivité et la viscoélasticité linéaire. En comparant ces données à la littérature de référence sur les hydrogels à base d'acrylamide-*co*-acide acrylique (sans nanoparticules), on a été constaté que Laponite® augmentait l'ASE et la conductivité, mais diminuait la rigidité. Des interprétations quantitatives ont été entreprises à l'aide de modèles théoriques pour l'ASE et la conductivité.

La diminution de la rigidité avec le dopage Laponite® est à l'encontre contraste avec de nombreuses études sur les hydrogels à base de poly(acrylamide) et poly(acide acrylique) dopés Laponite®. Cela semble refléter un degré élevé de neutralisation de l'acide acrylique, qui favorise la répulsion électrostatique entre la Laponite® et le réseau polymère, transformant ainsi la Laponite® en une charge nano-particulaire beaucoup plus passive à pH neutre. Cette observation peut avoir des implications technologiques bénéfiques, par exemple, elle favorise la libération de NP. D'autres informations ont été obtenues en comparant les hydrogels polymères avec leurs homologues en solution de monomère, permettant d'examiner plus en détail les effets de la polymérisation et de la réticulation.

Acknowledgements

I have received considerable support and assistance throughout my master's studies at McGill University.

Firstly, I would like to express my deepest gratitude to my parents for their understanding, support, and unconditional love. I wouldn't be able to reach this far without them.

Many thanks go to my supervisor, Professor Reghan J. Hill, for offering invaluable support, advice, guidance, and encouragement throughout my master's study at McGill. I am grateful for financial support from a stipend and nominations leading to Eugenie Ulmer-Lamothe (EUL) Scholarships and Graduate Excellence Awards. In addition, Prof. Hill's precise editing and insightful feedback contributed tremendously to the production of this thesis. I am proud of and grateful for my time working with Prof. Hill.

My thanks also go to past and present members of Prof. Hill's research group: Dr. Gbolahan Afuwape, Mr. Adel Al-Amodi, Mr. Amir Sina Nassirian, Ms. Sahar Jafari Daghalian Sofla, and especially Ms. Olawunmi Odunola, who trained me to use the rheometer and electrokinetic sonic amplitude analyzer, and provided useful advice on my experimental plans, heart-warming support, and care.

I would also like to acknowledge Mr. Frank Caporuscio for the gas cylinder, waste disposal, reverse osmosis water trainings, and other technical support, and Mr. Ranjan Roy for assistance with a critical air-filter change and other technical support.

I would like to express my thanks to friends and other family members, especially to Miss. Jiyu Tian, who has been always on my side, encouraging and supportive throughout my master’s studies. I cannot be more grateful to have her as my best friend.

Finally, I would like to acknowledge the NSERC Discovery and Research Tools and Instruments grants that supported this research, Eugenie Ulmer-Lamothe (EUL) Graduate Scholarship, and Graduate Excellence Awards.

Preface

This manuscript-based thesis is written in accordance with McGill's Guidelines for Thesis Preparation. It contains one manuscript (Chapter 3) in preparation for submission to a peer-reviewed journal.

- J. Wu (main author): Wrote initial drafts of all chapters with corrections provided by the thesis supervisor; designed and performed the experiments and data analysis in Chapter 3.
- R. J. Hill (thesis supervisor): Supervised the research, assisted experimental design, data analysis and interpretation; revised the thesis; developed the theory in Chapter 3.

Contents

List of figures

List of tables

Chapter 1

Introduction

1.1 Motivation

The inspiration for studying the mobility of nanoparticles in polyelectrolyte hydrogels in this thesis comes from the question of how nanoparticles travel through body tissues and reach the brain. As highlighted in a CBC documentary, nano-sized metal particles found in human brains might be from air pollution, which could potentially damage the brain (The Nature of Things: You can't see it but it can kill you. Air pollution hurts more than our lungs, CBC Docs, 2019) [Maher et al., 2016]. Another study conducted by Raliya et al. [2017] also reported that aerosols made of heavy metal nanoparticles (gold) presented to a peripheral sensory organ (*i.e.*, insect antenna) were transported to the brain within an hour. According to Raliya et al. [2017], further studies that focus on the "particle mode of entry, efficacy of delivery, transport mechanisms, and long term toxicity" are necessary to fulfill results presented in their study. As a foundational step toward understanding how nanoparticles travel through body tissues, this thesis studies the mobility of nanoparticles in polymer hydrogel based on polymer hydrogels sharing similarities in mechanical properties and spatial structure with natural soft tissue [Slaughter et al., 2009, Zhang and Khademhosseini, 2017, Lee et al., 2020].

Another motivation of studying nanoparticles in hydrogels is from the variety of applications of nanocomposite hydrogels in biomedical fields and wastewater treatment. Applications in biomedical fields include bio-sensors, actuators, drug delivery, stem cell engineering, regenerative medicine, and other biomedical devices [Gaharwar et al., 2014]. With the introduction of nanoparticles to hydrogel networks, the resulting nanocomposite hydrogels can be engineered to possess superior physical, chemical, electrical, and biological properties [Gaharwar et al., 2014]. In terms of wastewater treatment, nanocomposite hydrogels have been used for toxic pollutant remediation due to their swellability, hydrophilicity, high adsorption capacities, *etc*. [Kurecic and Smole, 2012]

While the properties of polymers and nanoparticles have been studied extensively, few studies have tested hypotheses on how certain types of nanoparticles and functional coatings interact with various types of gel [Zhao et al., 2020]. One of the challenges of studying the nanoparticle-hydrogel interactions is to apply common diagnostic methods, *e.g.*, light scattering and centrifugation techniques for particle size distribution and electrical characteristics [Bhosale et al., 2011]. These methods are limited by sample opacity and the extra layer of complexity introduced by nanoparticles. Electroacoustic characterization, provides microstructural insight by registering the electrokinetic sonic amplitude (ESA) and dynamic mobility of concentrated opaque materials [Bhosale et al., 2011]. Although electroacoustic spectroscopy was commercialized for colloidal dispersions, it has been applied in recent years to other viscoelastic networks, such as hydrogels and uncharged nanoparticle-doped hydrogels, and charged hydrogels without nanoparticle inclusions [Adibnia et al., 2020]. Although the effect of charge on the electroacoustic responses of polymer hydrogels has been studied, it is unknown how the electroacoustic response is affected by charged nanoparticles [Adibnia et al., 2020]. Therefore, this thesis applies electroacoustic characterization to nanoparticle-doped charged polyelectrolyte hydrogels.

1.2 Objectives

The overall objective of this thesis is to build a foundational understanding of the electroacoustic response (ESA) and mobility of Laponite® nanoparticles in charged poly(AAm-*co*-AAc) hydrogels. This was pursued by seeking answers to the following questions:

- What are the electroacoustic responses, electrical conductivity, and dynamic mobility of Laponite® nanoparticle-doped charged poly(AAm-*co*-AAc) hydrogels?
- Can the theory developed by Adibnia et al. [2020] on poly(AAm-*co*-AAc) hydrogels without nanoparticles be applied to Laponite® nanoparticle-doped poly(AAm-*co*-AAc) hydrogels?
- What is the effect of varying charge density and varying nanoparticle concentration on the electroacoustic responses, electrical conductivity, and dynamic mobility of Laponite® nanoparticle-doped charged poly(AAm-*co*-AAc) hydrogels?
- What is the effect of polymerization and cross-linking on the electroacoustic responses, electrical conductivity, and dynamic mobility of Laponite® nanoparticle-doped charged poly(AAm-*co*-AAc) hydrogels?
- What is the effect of introducing Laponite® nanoparticles to poly(AAm-*co*-AAc) hydrogels in terms of mechanical (viscoelastic) properties?

Bibliography

V. Adibnia, G. Afuwape, and R. J. Hill. Electrokinetic sonic amplitude of polyelectrolyte solutions and networks. *Macromolecules*, 53:7460–7468, 2020.

P. S. Bhosale, J. Chun, and J. C. Berg. Electroacoustics of particles dispersed in polymer gel. *Langmuir*, 27(12):7376–7379, 2011.

A. K. Gaharwar, N. A. Peppas, and A. Khademhosseini. Nanocomposite hydrogels for biomedical applications. *Biotechnol. Bioeng.*, 111(3):441–453, December 2014.

M. Kurecic and M. S. Smole. Polymer nanocomposite hydrogels for water purification. In F. Ebrahimi, editor, *Nanocomposites-New Trends and Developments*. IntechOpen, 2012.

M. Lee, R. Rizzo, F. Surman, and M. Zenobi-Wong. Guiding lights: Tissue bioprinting using photoactivated materials. *Chem. Rev.*, 120(19):10950–11027, 2020.

B. Maher, I. Ahmed, V. Karloukovski, D. MacLaren, P. Foulds, D. Allsop, D. Mann, R. Torres-Jardón, and L. Calderon-Garciduenas. Magnetite pollution nanoparticles in the human brain. *Proc. Natl. Acad. Sci. U.S.A.*, 113(39):10797–10801, 2016.

R. Raliya, D. Saha, T. Chadha, B. Raman, and P. Biswas. Non-invasive aerosol delivery and transport of gold nanoparticles to the brain. *Sci. Rep.*, 7, 2017.

B. V. Slaughter, S. S. Khurshid, O. Z. Fisher, A. Khademhosseini, and N. A. Peppas. Hydrogels in regenerative medicine. *Adv. Mater.*, 21(32-33):3307–3329, 2009.

Y. S. Zhang and A. Khademhosseini. Advances in engineering hydrogels. *Science*, 356 (6337), 2017.

H. Zhao, M. Liu, Y. Zhang, J. Yin, and R. Pe. Nanocomposite hydrogels for tissue engineering applications. *Nanoscale*, 12:14976–14995, 2020.

Chapter 2

Literature review

2.1 Hydrogel nanocomposites

Hydrogels are cross-linked polymer networks swollen with a large amount of water [Rafieian et al., 2018, Schexnailder and Schmidt, 2009]. Common materials that form hydrogels vary from synthetic polymers *e.g.*, polyethylene-oxide (PEO), polyvinyl-alcohol (PVA), polyacrylamide (PAAm), poly(acrylic acid) (PAAc) *etc.*, to naturally derived polymers, *e.g.*, agarose, alginate, chitosan, collagen *etc.* [Afuwape, 2021] The synthesis of hydrogels involves physical and/or chemical cross-linking, where physical cross-linking is formed via intermolecular interactions, *e.g.*, hydrogen bonds, electrostatic interactions, hydrophobic interactions, *etc.*, which are often reversible. In the case of chemical cross-linking, the network is formed by covalent bonds via chemical reactions, *e.g.*, between polymers or between polymers and cross-linkers, or via free radical polymerization, and so are irreversible [Batista et al., 2019, Wang et al., 2020]. Hydrogels bear the advantages of being biocompatible, biodegradable, and are capable of conformational change. These properties enable them to be scaffolds for and mimic the properties of living tissues [Singh et al., 2014, Hamidi et al., 2008, Mantha et al., 2019]. The stimuli-responsive properties and self-heading capabilities of hydrogels have also attracted research interest in biomedical and tissue engineering [Li et al., 2020]. However, hydrogels are often limited by their poor mechanical strength and low toughness [Singh et al., 2014].

Studies have established that introducing nanomaterials with high surface area-to-volume and aspect ratio into hydrogels can improve mechanical properties [Xing and Tang, 2021, Sasaki and Akiyoshi, 2010]. Some examples of nanomaterials include, but are not limited to, carbon-based nanomaterials, *e.g.*, carbon nanotubes or CNTs, graphene, and nanodiamonds; polymeric nanoparticles, *e.g.*, dendrimers and hyper-branched polymers; inorganic/ceramic nanoparticles, *e.g.*, hydroxyapatite, silicates, and calcium phosphate; and metal/metaloxide nanoparticles, *e.g.*, gold, silver and ironoxides [Rafieian et al., 2019]. After introducing nanomaterials, hydrogel nanocomposites have been demonstrated to be smart drug carriers, targeting sites with efficient transport and controlled release [Fratoddi et al., 2019, Merino et al., 2015].

Laponite® XLG, one of the inorganic nanoparticles, is an appealing nanofiller due to its unique structure (disc-shaped) and charging (negatively charged faces and positively charged edges). Laponite® nanoparticles are very thin (1 nm in thickness) disks ($20-30$ nm in diameter), used as a rheology modifier (thickening agent) in coatings, paints, and personal care products [Becher et al., 2019]. As a thickening agent, Laponite® suspensions can become very viscous at very low nanoparticle volume fractions, achieving viscosities several orders of magnitude higher than that of the solvent (water) [Zhao et al., 2020]. The addition of Laponite® to hydrogels often significantly enhances mechanical properties [Zhao et al., 2020]. From an environmental perspective, Laponite® nanoparticles are considered non-toxic, biodegradable, and biocompatible, as they degrade to non-toxic components under acidic conditions [Becher et al., 2019]. These make Laponite® a promising nanofiller for hydrogels.

In terms of polymer selection, polyacrylamide (PAAm)-Laponite® hydrogel nanocomposites have been studied extensively [Zhu et al., 2006, Okay and Oppermann, 2007, Adibnia et al., 2017, Liu et al., 2020]. Zhu et al. [2006] found that the Laponite®/PAAm hydrogel nanocomposites showed excellent resilience, low hysteresis, high tensile strength, and ultra-high elongation. Another commonly used polymer is polyacrylic acid (PAAc) or its sodium salt [Labanda and Llorens, 2004, 2005, Atmuri and Bhatia, 2013, Shen et al., 2014, Becher et al., 2019], where the resulting Laponite®/PAAc hydrogel nanocomposites have been demonstrated to be self-standing, moldable, robust, and with shear-shining and self-healing bahaviour [Becher et al., 2019]. Other options are poly(N-isopropylacrylamide) (PNIPAM)-based Laponite®-doped hydrogels [Zhu et al., 2006, Wang et al., 2012, Kohl, 2020], and poly(ethylene oxide) (PEO)-based Laponite®-doped hydrogels [Nelson and Cosgrove, 2004, Schexnailder and Schmidt, 2009].

Since the hydrogel nanocomposites formed from a single monomer have studied adequately, this thesis seeks to study copolymer hydrogels from PAAm and PAAc, as inspired by the electroacoustic responses of charged hydrogels by Adibnia et al. [2020]. They found that a weakly charged hydrogels register a negative real part of the ESA, changing sign at higher PAAc contents. According to their mechanistic theoretical model, the ESA sign change can be attributed to the hydrodynamic friction, charge, and inertia of the network strands and mobile counterions.

2.2 Development of electroacoustic spectroscopy

The theoretical development of electroacoustic effects can be traced to Debye [1933] who first derived the colloid vibration potential (CVP), which arises from the alternating electric field generated from a sound wave passing through an electrolyte (colloid in this case). However, it was very difficult to measure tiny voltages until the commercialization of two CVP devices. One of the devices, developed by Matec Applied Sciences, measures the converse of the CVP, which is termed the electrokinetic sonic amplitude (ESA) [Oja et al., 1985].

O'Brien [1988] undertook the first step toward theoretical interpretation of the ESA, showing that electroacoustic measurements can be used for particle dynamic mobility determination, also deriving a formula that links the dynamic mobility to particle size and ζ-potential. In the next 6 years, the colloids group at the University of Sydney developed the AcoustoSizer, which is capable of determining the size distribution and zeta potential in a suspension of arbitrary concentration [O'Brien et al., 1995].

A modern AcoustoSizer instrument and schematic of its cell are shown in Figure 2.1. A pulse of alternating voltage is generated from the two electrodes on the inner sides of the two glass rods. This voltage creates an electric field, so that the charged particles in the colloid generate an ultrasound pressure from their electrophoretic motion. This ultrasound wave then travels through both sides of the glass rods to be detected by the transducer as the ESA signal [O'Brien et al., 1995].

Bibliography

V. Adibnia, K. W. Cho, and R. J. Hill. Nanoparticle Coupling to Hydrogel Networks: New Insights from Electroacoustic Spectroscopy. *Macromolecules*, 50(10):4030–4038, May 2017.

V. Adibnia, G. Afuwape, and R. J. Hill. Electrokinetic sonic amplitude of polyelectrolyte solutions and networks. *Macromolecules*, 53:7460–7468, 2020.

G. A. Afuwape. *Nanoemulsion-hydrogel composites: electro-kinetic dynamics, viscoelastic and swelling responses*. PhD thesis, McGill University, February 2021.

A. K. Atmuri and S. R. Bhatia. Polymer-mediated clustering of charged anisotropic colloids. *Langmuir*, 29:3179–3187, 2013.

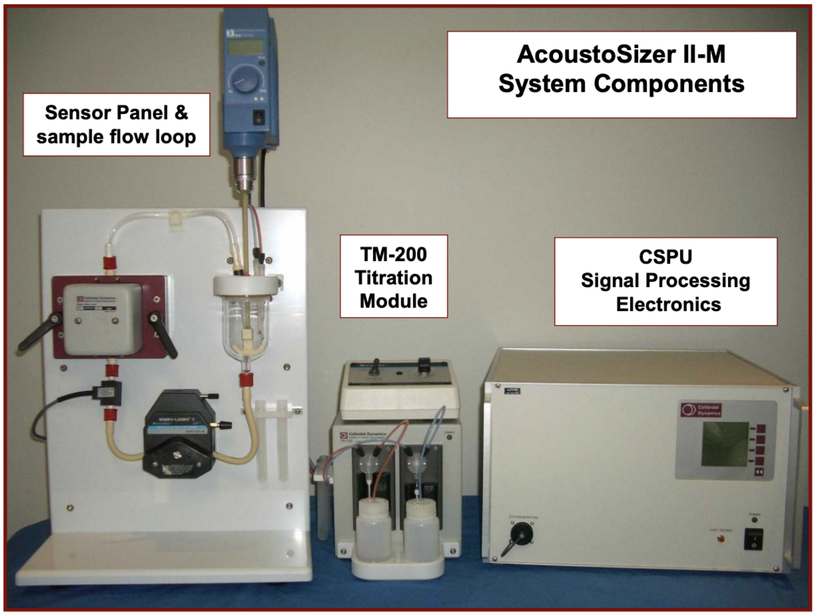

(a)

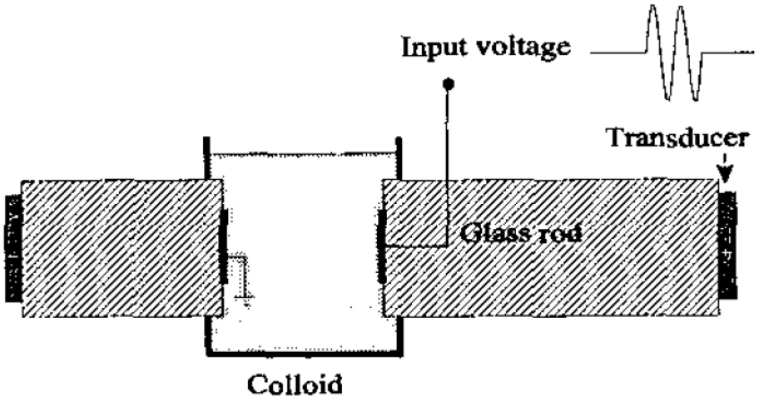

(b)

Figure 2.1: (a) Colloidal Dynamics, LLC AcoustoSizer II (from the instrument manual). (b) AcoustoSizer cell schematic (from O'Brien et al. [1995]).

R. A. Batista, C. G. Otoni, and P. J. Espitia. Chapter 3 - fundamentals of chitosan-based hydrogels: elaboration and characterization techniques. In A.-M. Holban and A. M. Grumezescu, editors, *Biomed. Mater. Eng.*, pages 61–81. Elsevier, 2019.

T. B. Becher, C. B. Braga, D. L. Bertuzzi, M. D. Ramos, A. Hassan, F. N. Crespilho, and C. Ornelas. The structure–property relationship in LAPONITE® materials: from Wigner glasses to strong self-healing hydrogels formed by non-covalent interactions. *Soft Matter*, 15(6):1278–1289, 2019.

P. Debye. A method for the determination of the mass of electrolytic ions. *J. Chem. Phys.*, 1(13), 1933.

I. Fratoddi, D. Lombardo, M. A. Kiselev, and M. T. Caccamo. Smart nanoparticles for drug delivery application: Development of versatile nanocarrier platforms in biotechnology and nanomedicine. *J. Nanomater.*, 2019.

M. Hamidi, A. Azadi, and P. Rafiei. Hydrogel nanoparticles in drug delivery. *Adv. Drug Deliv. Rev.*, 60(15):1638–1649, 2008.

K. Kohl. Comparison of Dynamic Light Scattering and Rheometrical Methods to Determine the Gel Point of a Radically Polymerized Hydrogel under Mechanical Shear. *Micromachines*, 11(5):462, Apr. 2020.

J. Labanda and J. Llorens. Rheology of laponite colloidal dispersions modified by sodium polyacrylates. *Colloids Surf. A Physicochem. Eng. Asp.*, 249:127–129, 2004.

J. Labanda and J. Llorens. Influence of sodium polyacrylate on the rheology of aqueous laponite dispersions. *J. Colloid Interface Sci.*, 289:86–93, 2005.

Z. Li, Y. Zhou, T. Li, J. Zhang, and H. Tian. Stimuli-responsive hydrogels: Fabrication and biomedical applications. *VIEW*, 2020.

X. Liu, X. Niu, Z. Fu, L. Liu, S. Bai, J. Wang, L. Li, Y. Wang, and X. Guo. A facile approach to obtain highly tough and stretchable laponites-based nanocomposite hydrogels. *Soft Matter*, 16:8394–8399, 2020.

S. Mantha, S. Pillai, P. Khayambashi, A. Upadhyay, Y. Zhang, O. Tao, H. Pham, and S. Tran. Smart hydrogels in tissue engineering and regenerative medicine. *Materials*, 12:3323, 10 2019.

S. Merino, C. Martín, K. Kostarelos, M. Prato, and E. Vázquez. Nanocomposite Hydrogels: 3D Polymer–Nanoparticle Synergies for On-Demand Drug Delivery. *ACS Nano.*, 9(5):4686–4697, 2015.

A. Nelson and T. Cosgrove. Dynamic light scattering studies of poly(ethylene oxide) adsorbed on laponite: layer conformation and its effect on particle stability. *Langmuir*, 20(24):10382–10388, Nov. 2004.

R. O'Brien, D. Cannon, and W. Rowlands. Electroacoustic determination of particle size and zeta potential. *J. Colloid Interface Sci.*, 173(2):406–418, 1995.

R. W. O'Brien. Electro-acoustic effects in a dilute suspension of spherical particles. *J. Fluid Mech.*, 190(71), 1988.

T. Oja, G. L. Petersen, and D. C. Cannon. Measurement of electro-kinetic properties of a solution. U.S. Patent 4,497,208, 1985.

O. Okay and W. Oppermann. Polyacrylamide-clay nanocomposite hydrogels: Rheological and light scattering characterization. *Macromolecules*, 40:3378–3387, 2007.

S. Rafieian, H. Mirzadeh, H. Mahdavi, and M. Masoumi. A review on nanocomposite hydrogels and their biomedical applications. *Sci. Eng. Compos.*, 26, 12 2018.

S. Rafieian, H. Mirzadeh, H. Mahdavi, and M. E. Masoumi. A review on nanocomposite hydrogels and their biomedical applications. *Sci. Eng. Compos.*, 26(1), 2019.

Y. Sasaki and K. Akiyoshi. Nanogel engineering for new nanobiomaterials: from chaperoning engineering to biomedical applications. *Chem. Rec.*, 10(6):366–376, 2010.

P. Schexnailder and G. Schmidt. Nanocomposite polymer hydrogels. *Colloid Polym. Sci.*, 287:1–11, 2009.

M. Shen, L. Li, Y. Sun, J. Xu, X. Guo, and R. K. Prud'homme. Rheology and adhesion of poly(acrylic acid)/laponite nanocomposite hydrogels as biocompatible adhesives. *Langmuir*, 30(6):1636–1642, Feb. 2014.

G. Singh, A. Lohani, and S. S. Bhattacharya. Hydrogel as a novel drug delivery system: a review. *J. Fundam. Pharm. Res.*, 2(1):35–48, 2014.

T. Wang, D. Liu, C. Lian, S. Zheng, X. Liu, and Z. Tong. Large deformation behavior and effective network chain density of swollen poly(N-isopropylacrylamide)–Laponite nanocomposite hydrogels. *Soft Matter*, 8(3):774–783, 2012.

W. Wang, R. Narain, and H. Zeng. Chapter 10 - hydrogels. In R. Narain, editor, *J. Surf. Sci. Nanotechnol.*, pages 203–244. Elsevier, 2020.

W. Xing and Y. Tang. On mechanical properties of nanocomposite hydrogels: Searching for superior properties. *Nano. Mater. Sci.*, 2021.

H. Zhao, M. Liu, Y. Zhang, J. Yin, and R. Pe. Nanocomposite hydrogels for tissue engineering applications. *Nanoscale*, 12:14976–14995, 2020.

M. Zhu, Y. Liu, B. Sun, W. Zhang, X. Liu, H. Yu, Y. Zhang, D. Kuckling, and H.-J. P. Adler. A novel highly resilient nanocomposite hydrogel with low hysteresis and ultrahigh elongation. *Macromol. Rapid Commun.*, 27:1023–1028, 2006.

Chapter 3

Nanoparticle-doped polyelectrolyte hydrogels

3.1 Abstract

Electroacoustic characterization of concentrated opaque materials provides micro-structural insight by registering the Electrokinetic Sonic Amplitude (ESA) and dynamic mobility. This characterization has been applied in recent years to uncharged nanoparticle-doped hydrogels and charged hydrogels without nano-particle inclusions, but not to charged hydrogels doped with charged nanoparticles. To understand the electroacoustic responses of these nano-composites, this study focuses on a series of Laponite® XLG-doped poly(acrylic acid-*co*-acrylamide) hydrogels, drawing on the ESA, electrical conductivity, viscoelastic rheology, and dynamic mobility. The hydrogel charge density is varied by the fraction of acrylic-acid monomer $f_{AAc} = c_{AAc}/(c_{AAc} + c_{AAm})$ while maintaining the total monomer concentration at $c_{AAc} + c_{AAm} = 8$ wt%. Laponite® concentrations $c_{Lap.}$ were maintained ≤ 1 wt%. Comparing the data from this study to those in the recent benchmark study of Adibnia et al. [2020] for charged hydrogels without nanoparticles, Laponite®-doping increased the electroacoustic signal and ionic conductivity, but decreased the hydrogel

storage modulus. Mechanistic theoretical models predicting how the real part of the ESA and ionic conductivity of polyelectrolyte hydrogels depend on f_{AAc} were extended to Laponite®-doped hydrogels, together furnishing an estimate of the partial molar volume of acrylamide (in polymer form) that is close to the value for pure acrylamide (based on its density and molecular weight). The generally lower storage modulus with Laponite®-doping contrasts with previous studies of Laponite®-doped PAAm and PAAc hydrogels and solutions. This seems to reflect the high degree of neutralization, which transforms the attraction between protonated carboxyl moieties and Laponite® to an electrostatic repulsion. The hindering effects of polymerization and cross-linking on acrylic acid-*co*-acrylamide networks were also investigated by comparing the ESA and conductivity of hydrogels with their monomer-solution counterparts.

3.2 Introduction

Polymeric hydrogel nano-composites have received considerable attention in tissue engineering due to desirable mechanical properties and other unique (*e.g.*, self-healing, antibacterial, antioxidation, *etc.*) [Schexnailder and Schmidt, 2009]. Specifically, hydrogel nano-composites have been termed 'smart' drug carriers, in the case of this research, pH-responsive hydrogels, targeting sites with efficient transport and controlled release of therapeutic drugs [Merino et al., 2015]. Introducing nanoparticles or nanostructures has overcome well-known limitations of hydrogels (*e.g.*, poor mechanical strength [Singh et al., 2014]). Therefore, combining the advantages of hydrogels (*e.g.*, flexibility, biocompatibility, and biodegradability) with improved mechanical strength from nanofillers, polymeric hydrogel nano-composites have been distinguished by extraordinary mechanical, optical, swelling/de-swelling properties [Haraguchi et al., 2007].

Nevertheless, the complex microstructure of hydrogel networks and the opacity of their nano-composites makes the application of common diagnostic methods (such as light scattering and centrifugation, which often require both low concentration and high optical transparency) challenging [Bhosale et al., 2011]. The addition of nanoparticles increases microstructural complexity, making it difficult to predict nano-composite properties from knowledge of the individual component properties [Danielsen et al., 2021]. Moreover, it is still not possible to test mechanistic hypotheses on how nanoparticles and functional coatings interact with gels and tissues [Zhao et al., 2020], although the properties of polymers and nanoparticles have been studied extensively.

Electroacoustic characterization provides microstructural insight by registering the Electrokinetic Sonic Amplitude (ESA) and dynamic mobility of concentrated opaque materials [Bhosale et al., 2011]. Although electroacoustic spectroscopy was commercialized for colloidal dispersions, it has been applied in recent years to uncharged nanoparticle-doped hydrogels, and charged hydrogels without nanoparticle inclusions [Adibnia et al., 2020]. In their study of the electroacoustic response of charged hydrogels, Adibnia et al. [2020] found that weakly charged hydrogels register a negative real part of the ESA, changing sign at higher charge densities. According to their mechanistic theoretical model, the ESA sign change can be attributed to hydrodynamic friction, charge, and inertia of the network strands, and mobile ions.

Common nanoparticles used to modify polymer hydrogels are carbon-, polymeric-, inorganic- and metallic-based [Pereira et al., 2020]. Among these, one of the synthetic silicates (inorganic-based nanoparticles), Laponite® is an attractive model example. Okay and Oppermann [2007] found that polyacrylamide (PAAm) is strengthened by Laponite®[1]. PAAm and its hydrogels have been commonly investigated as flocculants for wastewater treatment [Kurenkov et al., 2002, Xiong et al., 2018, Ngema et al., 2020] and drug-delivery dressing materials [Srivastava et al., 2014, Sabbagh and Muhamad, 2017, Singh et al., 2021]. With the addition of Laponite®, PAAm-based Laponite®-doped hydrogels have

---

[1] $(\mathrm{Na}^{+}_{0.7}[\mathrm{Si}_8\mathrm{Mg}_{5.5}\mathrm{Li}_{0.3})\text{-}\mathrm{O}_{20}(\mathrm{OH})_4]^{-}_{0.7}$

been studied as an inexpensive, super-absorbent hydrogel for cationic dye in wastewater treatment [Yi and Zhang, 2008, Zhang et al., 2012, Li et al., 2008].

Laponite® (XLS and XLG) nanoparticles are very thin (1 nm) disk-shaped, synthetic crystalline colloids (20–30 nm diameter), bearing negative charge on the faces, and positive charge on the edges [Cummins, 2007]. This unique charging provides Laponite® edge-rim electrostatic attraction, resulting in a physical, reversible edge-rim binding. This endows Laponite® dispersions with shear-thinning rheology, by which colloidal networks are temporarily broken when sheared [Sheikhi et al., 2018].

Laponite® NPs have been used as rheology modifiers (thickening agents) in coatings, paints, and personal care products [Becher et al., 2019]. As a thickening agent, Laponite® suspension viscosities with very low nanoparticle volume fractions can be several orders of magnitude higher than of the solvent (water) [Zhao et al., 2020]. The addition of Laponite® to hydrogels often significantly enhances mechanical properties [Ling et al., 2017]. From an environmental perspective, Laponite® is considered non-toxic, biodegradable, and biocompatible, because it degrades into non-toxic components under acidic pH [Becher et al., 2019].

PAAm- and PAAc-based Laponite® hydrogel nano-composites (poly(AAc-*co*-AAm) hydrogels) with or without organic cross-linkers have been investigated as dye absorbents [Aalaie and Youssefi, 2011, Sediiki et al., 2020, Chen et al., 2013]. Other fields of application of PAAm-PAAc based polyelectrolytes include wastewater treatment [Radoiu et al., 2004], heavy metal removal [Zhang, 2009, Çavuş et al., 2009], and biomedicine [Becerra-Bracamontes et al., 2007].

Shen et al. [2014] synthesized a series of Laponite®-doped PAAc hydrogels, some of which were concentrated PAAc solutions physically cross-linked by Laponite®, showing that their viscosity, storage modulus, and loss modulus increased significantly upon increasing the Laponite® and PAAc concentrations, but decreased when increasing the degree of AAc neutralization with pH $= 3.64$–4.68. They attributed the enhanced mechanical properties to hydrogen bonding of protonated carboxyl groups at the prevailing pH values.

In this study, poly(AAc-*co*-AAm) hydrogels and their AAc-*co*-AAm monomer-solution counterparts are doped with Laponite® (XLG). According to Liu et al. [2020], poly(acrylic acid) is expected to adsorb onto the positively charged edges of Laponite® disks, so the "house of cards? structure is expected to vanish when Laponite® (XLG) is in the presence of AAc^{-}.

3.3 Materials and methods

Materials

Chemicals used in this study are 99 wt% anhydrous acrylic acid (AAc, contains 200 ppm MEHQ as inhibitor), and sodium metabisulfite ≥ 99 %, (SMBS, powder), purchased from Sigma-Aldrich; 40 wt% acrylamide (AAm, aqueous solution), 2 wt% N,$N\prime$-methylenebisacrylamide (NMBA) (aqueous solution), and ammonium persulfate (APS, power, electrophoresis grade), purchased from Fisher Scientific; N,N,N′,N′-tetramethylethylenediamine (TEMED, 99 %), purchased from GE Healthcare Life Science, Germany; and Laponite® XLG (powder), generously provided by BYK Additives and Instruments.

Laponite® stock solution

A Laponite® stock solution was prepared by dispersing 1.2 g of Laponite® XLG in 40 mL of reverse-osmosis (RO) water to form a 3 wt% dispersion. Dispersion comprised two steps: initial dispersion using a vortex mixer, and secondary dispersion using a Sonicator. As Laponite® particles generally contain ≈ 15 wt% moisture at 50 % relative humidity [Valencia et al., 2018], the actual Laponite® concentration in the stock solution is estimated ≈ 2.55 wt%. During the initial dispersion, the mixture was vigorously stirred for ≈ 2 min using a vortex mixer, forming a white, opaque liquid. This Laponite® solution was then transferred to a 50 mL beaker and sonicated for 5 min using a Qsonica Q500 Sonicator (at 70 % maximum amplitude, paused for 2 s every 5 s) for the secondary dispersion. This transformed the mixture to transparent, colorless liquid. However, due to the "house of cards" structure, and possibly aggregates formed by Laponite® XLG nanoparticles, this stock solution became opaque, viscous and gel-like in several hours. The Laponite® stock solution was therefore vigorously stirred for $\gtrsim 1$ min using a vortex mixer to "de-gel" before further use.

Synthesis of nanoparticle-doped polyelectrolyte samples and titration (precursor solution)

The total monomer concentration (acrylic acid AAc and acrylamide AAm) for all samples in this study was fixed to ≈ 8 wt%. Three sets of samples were synthesized. One is Laponite®-doped poly(AAm-*co*-AAc) hydrogels with AAc monomer fraction $f_{AAc} = 0$–1, maintaining a fixed Laponite® concentration ≈ 0.85 wt%. The chemical cross-linker (NMBA) concentration was maintained with a ratio $1/19$ of the total monomer concentration ($8/19 \approx 0.42$ wt%). The precursor solution, containing monomers, Laponite® and NMBA, was titrated (Metrohm 809 Titratando)) with ≈ 4.17 M NaOH solution (as used by Adibnia et al. [2020]) to achieve pH ≈ 7. Following titration, APS was added as initiator, achieving a concentration ≈ 4.38 mM [Adibnia et al., 2020]. Nitrogen gas was then bubbled through all samples for 5 min to remove dissolved oxygen. SMBS was then added as catalyst, achieving a concentration ≈ 5.26 mM [Adibnia et al., 2020]. Note that TEMED was added only to samples without AAc (immediately after adding SMBS), achieving a concentration ≈ 1 μg mL^{-1}. Upon the addition of SMBS, precursor solutions begin to polymerize and cross-link. A schematic of the hydrogel nano-composite synthesis is shown in Figure 3.1. According to, e.g., Liu et al. [2020] and Shen et al. [2014], the "house of cards" structure vanishes when in the presence of other charged species, such as AAc^{-} in this case. However, potential aggregations between Laponite® and copolymer

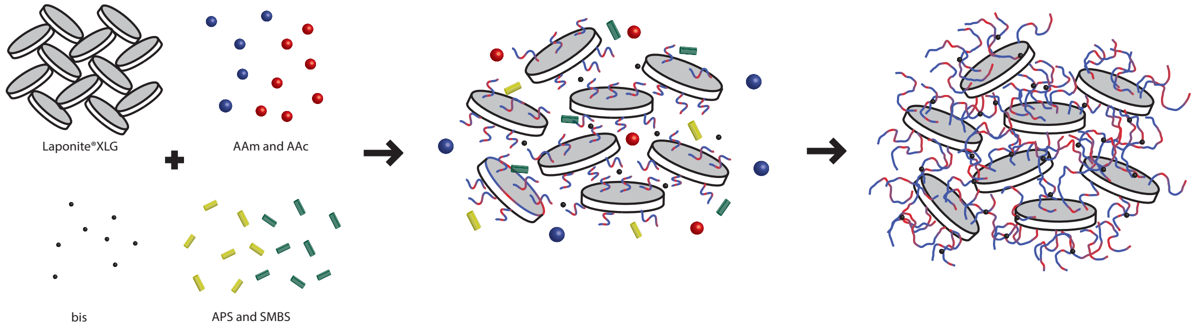

Figure 3.1: Schematic of hydrogel nano-composite synthesis involving *in situ* free-radical polymerization and cross-linking at room temperature. Note that AAc neutralization with NaOH is undertaken on the entire mixture, prior to initiating polymerization and cross-linking.

is likely to happen. Therefore, although not within the scope of this thesis, it might be necessary to apply structural or spacial characterizations in the future studies, *e.g.*, X-ray diffraction and dynamic light scattering characterizations, to ensure the well dispersion of nanoparticles in copolymer. The pre-gel solution was quickly transferred to either the ESA instrument (using a syringe) or to the rheomemeter (using a pipette).

For example, a pre-gel sample with $f_{AAc} = 0.5$ contains 10 mL of Laponite® stock solution, 6.32 mL of NMBA solution, 3 mL of AAm, 1.212 mL of AAc, 0.3 mL of 10 wt% APS solution, 0.3 mL of 10 wt% SMBS solution, and was titrated with ≈ 3.8 mL of 4.17 M NaOH. RO water was then added to bring the total volume to 30 mL. As shown in Figure 3.2, the pre-gel solution and hydrogel appeared cloudy. Although some bubbles remain in the hydrogels after bubbling N_2 through the pre-gel solution, a comparison of ESA and conductivity for samples with and without and ostensible bubble excess (by vigorously shaking the pre-gel solution before injection into the ESA sample holder), demonstrated that bubbles from N_2 degassing do not significantly impact these measurements.

The second set of samples were monomer solutions with $f_{AAc} = 0$–1 and $c_{Lap.} = 0.85$ wt%, but without NMBA, APS, SMBS or TEMD. Their precursor solutions were also titrated with 4.17 M NaOH to achieve pH ≈ 7. After neutralization, nitrogen gas was bubbled through to remove dissolved oxygen before transferring to the ESA instrument.

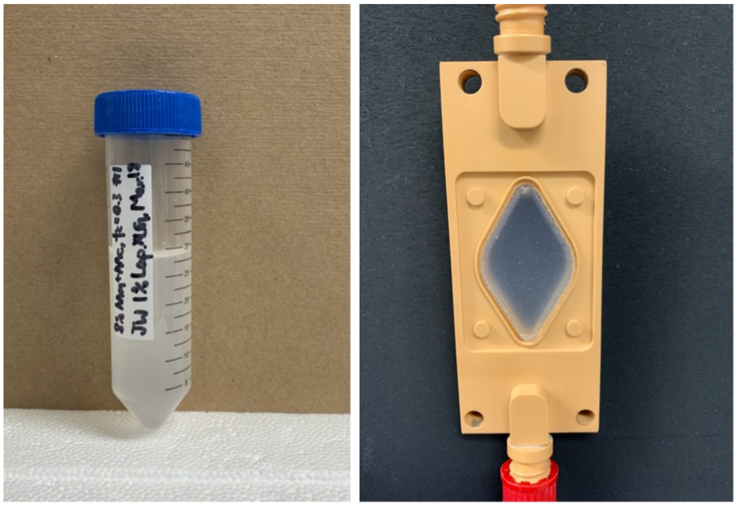
(a) (b)

Figure 3.2: Laponite®-doped poly(AAm-*co*-AAc): (a) Pre-gel solution and (b) polymerized and cross-linked (cast in the ESA cell).

The third set of samples were hydrogels with $c_{Lap.} = 0$–1 % and $f_{AAc} = 0.5$. These were prepared as the first set.

Note that hydrogels and monomer solutions with $f_{AAc} = 0$ were not neutralized. Such hydrogels registered pH $\approx 6.52 \pm 0.01$ (standard deviation from $n = 2$ sample replicates in the ESA instrument), and their monomer solutions (without NMBA, APS, SMBS, or TEMD) registered pH $\approx 7.00 \pm 0.01$ ($n = 2$).

Rheology

Rheological measurements were performed using an ARES-G2 (TA instruments) rheometer, adopting the same instrument procedures and settings as Adibnia et al. [2020]. Following nitrogen bubbling, catalyst (SMBS) was added to hydrogel precursor solutions, and quickly transferred to the bottom rheometer plate with the gap between the parallel plates set to 1 mm. Silicon oil (from Sigma-Aldrich Inc.) was deposited around the sample edges to prevent evaporation. Three types of test were performed in sequence on each sample (without opening the evaporation blocker): time series at strain $\gamma = 0.02$ and angular frequency $\omega = 1$ rad s^{-1} (3–6 h), strain sweeps with $\omega = 1$ rad s^{-1}, $\gamma = 0.001$–1; and frequency sweeps with $\gamma = 0.02$, $\omega = 0.1$–100 rad s^{-1}.

ESA, dynamic mobility and conductivity

Electrokinetic Sonic Amplitude experiments were performed using an Acoustosizer II (Colloidal Dynamics LLC) instrument, capable of measuring particle size (ranges from 0.02 to 10 μm), zeta-potential (on particles from 1 nm to 10 μm [Colloidal Dynamics, 2000]), pH, dynamic mobility, and conductivity of concentrated colloidal dispersions up to 40 vol %. Although the Acoustosizer II was commercialized for colloidal dispersions, it has been applied to hydrogels and monomer solutions [Adibnia and Hill, 2014]. Following the manufacturer's procedure, ESA measurements were undertaken following conductivity and ESA calibrations. About 35 ESA spectra were measured for each sample, including at least 5 steady-state measurements, each taking ≈ 4.5 min.

The ESA instrument measures the ultrasound pressure from electrophoretic motion of charged particles at MHz frequencies [Colloidal Dynamics, 2000]. The ESA signal depends on the particle charge and size. Since inertia depends on mass, particles with larger mass tend to register a phase lag. Other factors affecting ESA are captured by the theory of O'Brien et al. [2003]:

$$\text{ESA} = A(\omega)\frac{z_s z_g}{z_s + z_g}\phi\frac{\rho_p - \rho}{\rho}\mu_D, \tag{3.1}$$

where ϕ is the particle volume fraction, ρ_p is the particle density, and ρ is the solvent density; z_s and z_g are the acoustic impedance of the suspension and glass block, respectively. $A(\omega)$ is an instrumental pre-factor, which is determined from calibration, and is independent of the sample. To determine this pre-factor, it is necessary to measure the ESA spectrum of a colloid with a known dynamic mobility: a silico tungstate (KSiW) solution for which

$$\phi\frac{\rho_p - \rho}{\rho}\mu_D = -3.02 \times 10^{-9} K, \tag{3.2}$$

where K (S m^{-1}) is the measured conductivity [Colloidal Dynamics, 2000], and ϕ can be calculated using

$$\phi \frac{\rho_p - \rho}{\rho} = n \frac{m - \rho v}{\rho}, \tag{3.3}$$

where n is the number density, m is the ionic mass, and v is the partial molar volume [O'Brien et al., 2003].

The ESA is a complex-valued function, which may be expressed as

$$\text{ESA}^* = \frac{P}{E} = |\text{ESA}| e^{i\angle\text{ESA}} = \text{ESA}' + i\text{ESA}'', \tag{3.4}$$

where P and E are the complex-valued, harmonically oscillating pressure and electric field, respectively. $|\text{ESA}|$ and $\angle\text{ESA}$ are the magnitude and phase angle, provided by the instrument software based on its real and imaginary parts

$$\text{ESA}' = |\text{ESA}| \cos(\angle\text{ESA}) \tag{3.5}$$

and

$$\text{ESA}'' = |\text{ESA}| \sin(\angle\text{ESA}), \tag{3.6}$$

respectively.

Additional information, including electroacoustic theory and technical aspects of the instrument, principles of operation, and calibration, are provided by O'Brien et al. [1995].

The dynamic mobility μ_D is defined with a magnitude and argument

$$|\mu_D| = \frac{V_0}{E_0} \text{ and } \angle\mu_D = -\theta, \tag{3.7}$$

where E_0 is the magnitude of an applied sinusoidal electric field, and V_0 is the particle velocity amplitude with θ the phase lag between the particle velocity V_0 and the applied field E_0 [Colloidal Dynamics, 2000].

3.4 Varying AAm charge density, fixed Laponite® concentration

The effects of varying the AAm charge density on Laponite®-doped poly(AAc-*co*-AAm) hydrogels, and on Laponite®-doped AAc-*co*-AAm monomer solutions are examined from the ESA, conductivity and rheology with fixed Laponite® NP concentration $c_{Lap.} = 0.85$ % (shown ≈ 1 in all figures), varying the AAc charge fraction f_{AAc} in the range 0–1.

3.4.1 ESA

ESA time series, Argand diagram and spectra for Laponite®-doped poly(AAm-*co*-AAc) hydrogels are shown in Figure 3.3. The time series are at $f = 14.4$ MHz. Colors distinguish samples with f_{AAc} in the range 0–1, as identified by the abscissae in Figure 3.7.

The quantitative theoretical interpretation of the ESA at low frequency by Adibnia et al. [2020] is based on an analysis of the hydrodynamic friction and charge of weakly-charged network strands, giving

$$\text{ESA} = \frac{Q}{\rho} \frac{e f_{AAc}(c_{AAc} + c_{AAm})}{6\pi\eta} \frac{\chi_{Na}\Delta m_{Na}}{a_{Na}} \left[1 - \frac{(\chi^*_{AAc}/\chi_{Na})(\Delta m_{AAm}/\Delta m_{Na})}{(a_{AAm}/a_{Na})} \ln(1/f_{AAc})\right] \tag{3.8}$$

where the total polymer concentration $c_{AAc} + c_{AAm}$ is a prescribed constant. Here, Q is an instrumental factor that is sample and frequency dependent [Adibnia et al., 2020], ρ is the solvent density, η is the solvent viscosity, c_i are species concentrations (AAm, AAc and Na), χ_i are dimensionless constants defined by their electrophoretic mobilities, Δm_i are the relative masses, and a_i are hydrodynamic radii.

Steady-state values of ESA$'$ at $f = 1$ MHz, time-averaged from spectra for $t \approx 120$–150 min of gelation, are plotted versus the AAc fraction f_{AAc} in Figure 3.4. Similarly to the hydrogels of Adibnia et al. [2020], ESA$'$ registers weak negative values when $f_{AAc} \ll 1$, here transiting to positive values when $f_{AAc} \gtrsim 0.2$. The theory of Adibnia et al. [2020]

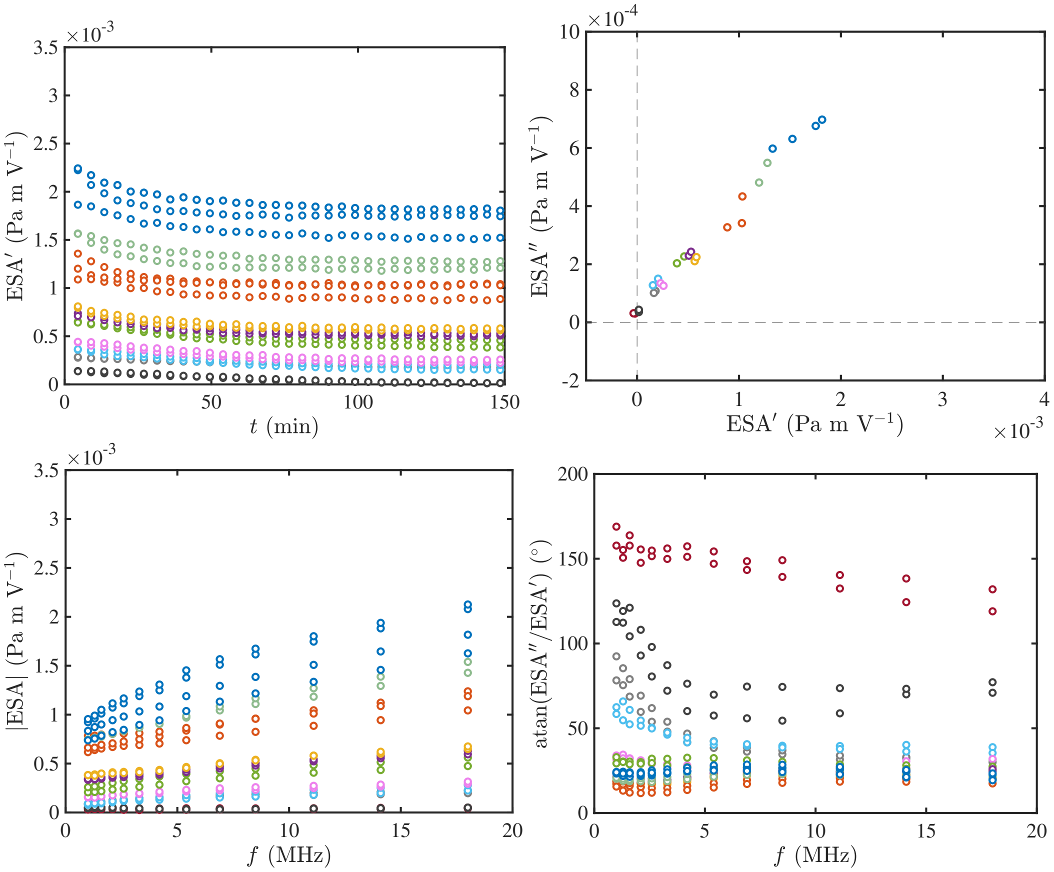

Figure 3.3: ESA data for neutralized Laponite®-doped poly(AAm-*co*-AAc) hydrogels with $c_{Lap.} \approx 1$ wt%. Top left: ESA′ time series ($f = 14.4$ MHz). Top right: Argand diagram (($f = 14.4$ MHz, time-averaged over $t = 135$–150 min). Bottom left: ESA magnitude spectra (time-averaged over $t = 135$–150 min). Bottom right: ESA phase-angle spectra (time-averaged over $t = 135$–150 min). Colors distinguish $f_{AAc} = 0$–1, as identified in the right panels of Figures 3.6 and 3.7.

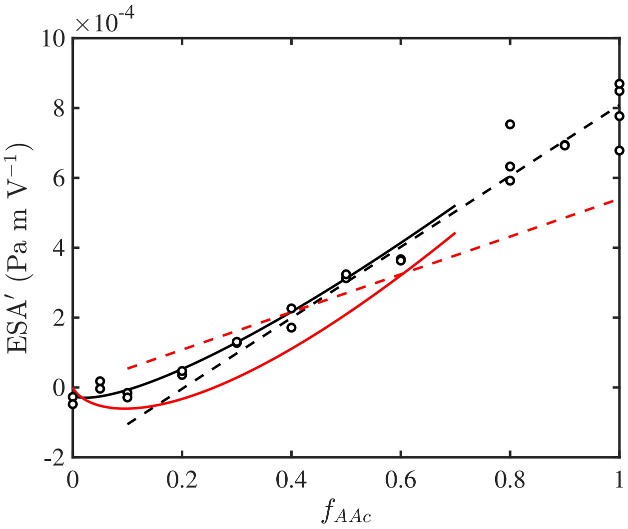

Figure 3.4: Theoretical model fits of Eqn. (3.13) (black) to steady-state ESA$'$ for neutralized Laponite®-doped poly(AAm-*co*-AAc) hydrogels with $c_{Lap.} \approx 1$ wt% at $f = 1$ MHz: Eqn. (3.15) (solid) and Eqn. (3.16) (dashed line). Red lines are the counterparts for hydrogels without nanoparticles ($c_{Lap.} = 0$) from Adibnia et al. [2020].

attributes ESA$'$ to the electrophoretic mobilities and concentrations of AAc$^-$ and Na$^+$ counter-ions, where the AAc$^-$ friction coefficient varies according to the linear charge density of the network strands, furnishing an effective hydrodynamic radius $a^*_{AAc} \sim a_{AAm}/f_{AAc}\text{ln}(1/f_{AAc})$.

For reference, it should be noted that ESA$' \sim -3 \times 10^{-4}$ Pa m V^{-1} for Laponite® in water, decreasing to ESA$' \sim -2 \times 10^{-4}$ Pa m V^{-1} in the presence of APS and SMBS (see the Appendix). Thus, when Laponite® is dispersed in poly(AAm-*co*-AAc) hydrogels, its own ESA is almost completely negated, while seeming to enhance ESA$'$ of the parent hydrogel, albeit in the positive direction. Possible reasons for this are examined as follows.

Fitting Eqn. (3.8) to these data (with low charge density) furnishes

$$\text{ESA}'(f = 1\text{ MHz}) \approx 9.0 \times 10^{-4} f_{AAc}[1 - 0.45\ \ln(1/f_{AAc})]\ \text{for}\ f_{AAc} \lesssim 0.4, \tag{3.9}$$

and a linear fit (passing through the origin) to the data with high charge density furnishes

$$\mathrm{ESA}'(f = 1\,\mathrm{MHz}) \approx 6.9 \times 10^{-4} f_{AAc} \text{ for } f_{AAc} \to 1. \tag{3.10}$$

Note that Eqn. (3.8) neglects the ESA of Laponite® and its counter-ions. Such an approximation may be justified by the hindered mobility of Laponite® NPs when they are embedded in the network, and/or the relatively low concentrations of NP counter-ions. Nevertheless, Eqns. (3.9) and (3.10) furnish different prefactors than reported by Adibnia et al. [2020] for the same hydrogels without Laponite® NPs:

$$\mathrm{ESA}'(f = 1\,\mathrm{MHz}) \approx 8.6 \times 10^{-4} f_{AAc}[1 - 0.74 \ln(1/f_{AAc})] \text{ for } f_{AAc} \lesssim 0.5, \tag{3.11}$$

and

$$\mathrm{ESA}'(f = 1\,\mathrm{MHz}) \approx 5.4 \times 10^{-4} f_{AAc} \text{ for } f_{AAc} \to 1. \tag{3.12}$$

These suggest that either the contributions of Laponite® NPs and their Na^+ and OH^- counter-ions to the ESA signal should not be neglected or that Laponite® NPs change the rheological properties of the hydrogel and/or mobilities of mobile ions.

According to Shahin and Joshi [2012], each Laponite® (RD) NP in water contributes up to ≈ 700 Na^+ counter-ions[2]. Therefore, from the density of Laponite® (2.53 g/cm^3), and dimensions of Laponite® disks (25 nm diameter, 1 nm thickness), the concentration of Na^+ counter-ions with $c_{Lap.} \approx 1$ wt% is ≈ 0.281 mM. It follows that the concentration of AAc^- counter-ions (Na^+) exceeds the concentration of Laponite® counter-ions (Na^+) when $f_{AAc} \gtrsim 2.4 \times 10^{-4}$. Thus, for all $f_{AAc} \neq 0$, the Na^+ concentration is dominated by the AAc^- counter-ions.

---

[2] Laponite® RD is reported by the manufacturer to have a lower purity than its XLS counterpart [Rockwood Additives Ltd, 2013].

Now consider modifying Eqn. (3.8) to include contributions from Laponite® NPs and their Na$^+$ and OH$^-$ counter-ions:

$$\begin{aligned}\text{ESA} &= \frac{Q}{\rho}\frac{ef_{AAc}(c_{AAc}+c_{AAm})}{6\pi\eta}\frac{\chi_{Na}\Delta m_{Na}}{a_{Na}}(1+\epsilon)\left[1-\frac{(\chi^*_{AAc}/\chi_{Na})(\Delta m_{AAm}/\Delta m_{Na})}{(1+\epsilon)(a_{AAm}/a_{Na})}\ln(1/f_{AAc})\right] \\ &+ \frac{Q}{\rho}\left(\frac{\chi_{NP}z_{NP}ec_{NP}\Delta m_{NP}}{6\pi\eta a_{NP}}-\frac{\chi_{OH}e\beta_{NP}c_{NP}\Delta m_{OH}}{6\pi\eta a_{OH}}\right), \qquad (3.13)\end{aligned}$$

where

$$\epsilon = \frac{-\alpha z_{NP}ec_{NP}}{f_{AAc}(c_{AAc}+c_{AAm})} > 0 \qquad (3.14)$$

is the ratio of the NP Na$^+$ counterion and AAc$^-$ counterion concentrations, and a_{NP} is the NP hydrodynamic radius, etc. Note that electroneutrality requires $z_{NP}e(1+\alpha-\beta)=0$, where αz_{NP} and βz_{NP} are, respectively, the number of Na$^+$ and OH$^-$ counter-ions per Laponite® NP with $z_{NP}e<0$ the net NP charge.

Despite its complex form, Eqn. (3.13) varies with respect to f_{AAc} in a manner that corresponds to adding a constant to Eqn. (3.8). Fitting this model to the data furnishes:

$$\text{ESA}'(f=1\,\text{MHz}) \approx 9.0\times10^{-4}f_{AAc}[1-0.35\ln(1/f_{AAc})]-2.37\times10^{-5} \text{ for } f_{AAc}\lesssim 0.4, \qquad (3.15)$$

and a linear fit (now with non-zero intercept) to the data with high charge density furnishes

$$\text{ESA}'(f=1\,\text{MHz}) \approx 9.9\times10^{-4}f_{AAc}-1.9\times10^{-4} \text{ for } f_{AAc}\gtrsim 0.4. \qquad (3.16)$$

Equations (3.15) and (3.16) are plotted in Figure 3.4 as black solid and dashed lines, respectively. The counterparts for hydrogels without Laponite® NPs from Adibnia et al. [2020] are shown in red. The negative sign of the constant in Eqn. (3.15) reflects a net contribution to the ESA from the (net negatively charged) Laponite® NPs and, possibly, their Na$^+$ and OH$^-$ counter-ions. The smaller pre-factor of the log term—0.35 compared to the value 0.74 from Adibnia et al. [2020] without Laponite®—suggests that Laponite® hinders the mobility (as measured by χ^*_{AAc}) or perhaps decreases the concentration of AAc$^-$ in the network, e.g., by association of AAc^- and Laponite®. Note that the pre-factor of the term that is linear in f_{AAc} is not affected by Laponite®, consistent with Laponite® NPs having no influence on the mobility of the AAc^- counterion (Na^+).

Finally, when $f_{AAc} \to 1$, the slope of the linear variation of ESA′ with respect to f_{AAc} increases by a factor of $9.9/5.4 \approx 1.8$ with the addition of Laponite® NPs. Again, this suggests that Laponite®-doping hinders the mobility and/or decreases the concentration of AAc^- in the network, thus increasing the net ESA from positive counter-ions (Na^+).

Comparison of neutralized Laponite®-doped AAm-*co*-AAc hydrogels and their monomer-solution counterparts

Further insights are gleaned from the ESA of neutralized AAm-*co*-AAc (monomer) solutions with 1 wt% Laponite® (here without initiator, chemical cross-linker or catalyst). ESA time series for such solutions are shown in Figure 3.5. Note that the axis limits are the same as for the poly(AAc-*co*-AAm) hydrogels in Figure 3.3. The magnitude of ESA′ is notably enhanced by an absence of cross-linking (and of cross-linking precursor ions), consistent with Adibnia et al. [2020] by which the ESA of neutralized monomer solutions decreased upon polymerization and cross-linking. Note that Adibnia et al. [2020] attributed the diminished ESA to a lower degree of ionization, and hindering of Na^+ mobility by the cross-linked network.

Steady-state ESA′ and ESA″ from Laponite®-doped poly(AAm-*co*-AAc) hydrogels and their Laponite®-doped monomer-solution counterparts are shown in Figures 3.6 ($f = 1$ MHz) and 3.7 ($f = 14.4$ MHz). These clearly demonstrate the significant degree to which polymerization and cross-linking decrease the ESA. Note the significantly different rates at which ESA increases with respect to f_{AAc}. Consistent with the theoretical model of Adibnia et al. [2020], the only samples with $f_{AAc} > 0$ that register $\text{ESA}' < 0$ are polymerized, cross-linked hydrogels at low frequency ($f = 1$ MHz) with $f_{AAc} \ll 1$.

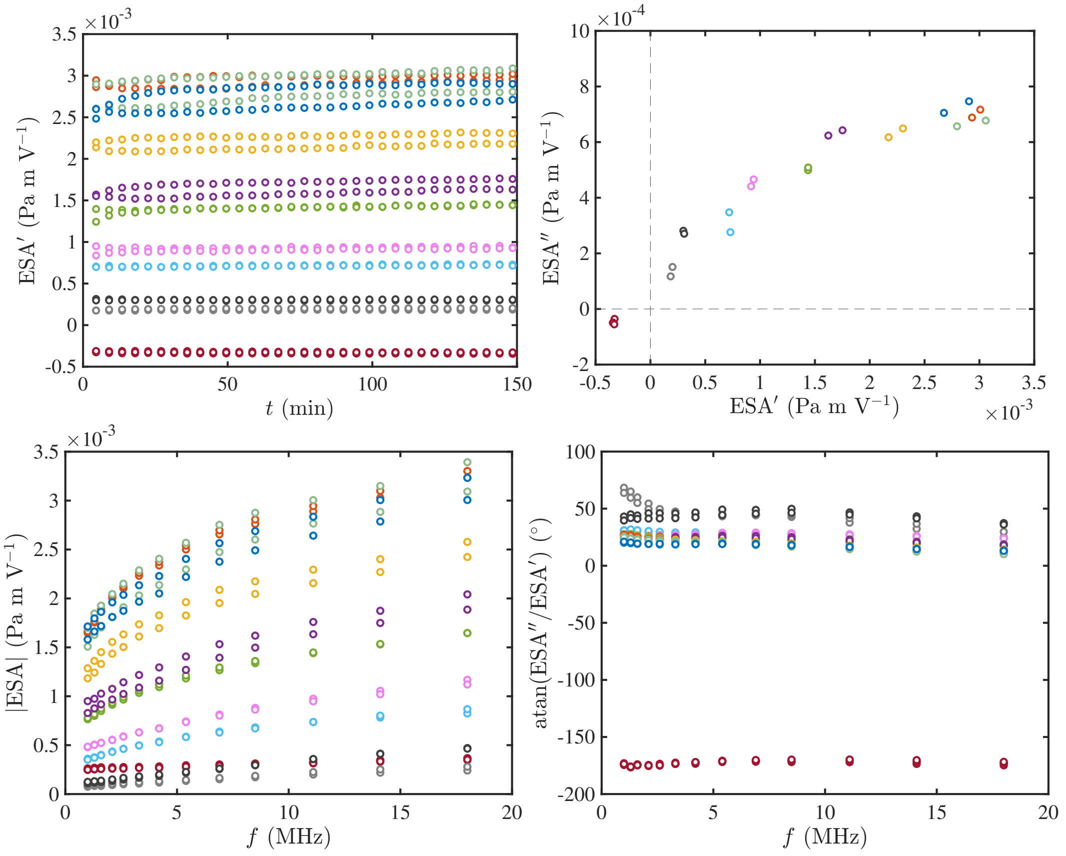

Figure 3.5: ESA data for neutralized Laponite®-doped poly(AAm-*co*-AAc) monomer solutions with $c_{Lap.} \approx 1$ wt%. Top left: ESA′ time series ($f = 14.4$ MHz). Top right: Argand diagram ($f = 14.4$ MHz, time-averaged over $t = 135$–150 min). Bottom left: ESA magnitude spectra (time-averaged over $t = 135$–150 min). Bottom right: ESA phase-angle spectra (time-averaged over $t = 135$–150 min). Colors distinguish $f_{AAc} = 0$–1, as identified in the right panels of Figures 3.6 and 3.7.

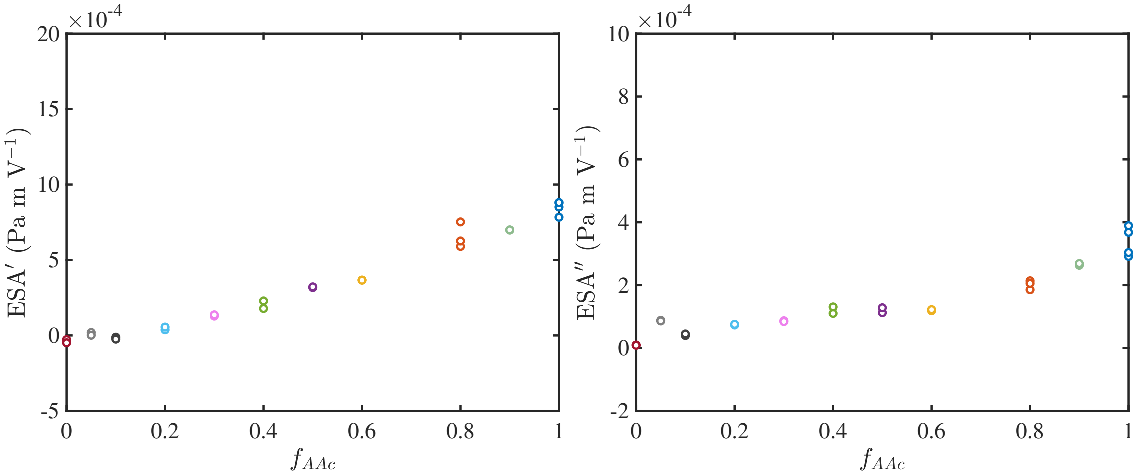

(a) poly(AAm-*co*-AAc) hydrogels.

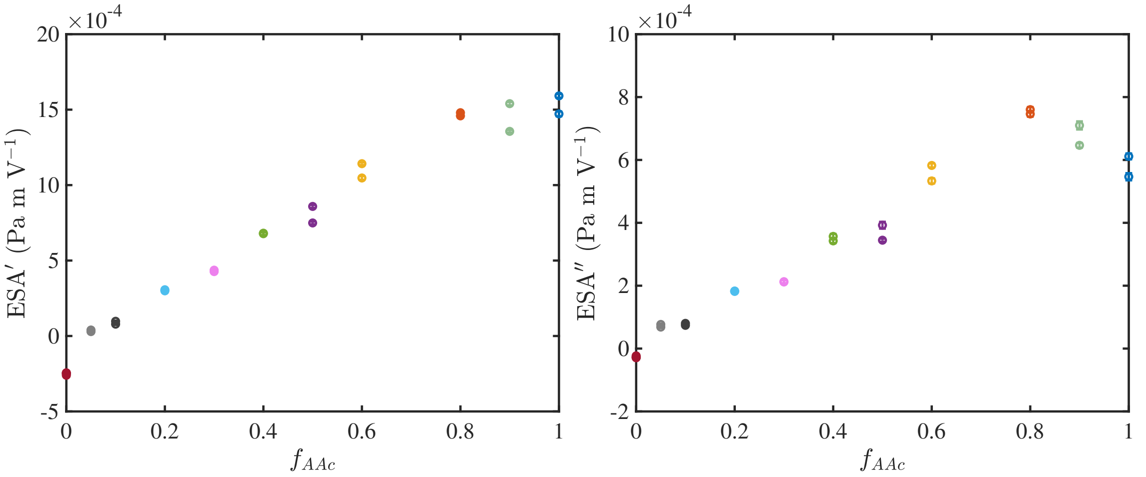

(b) AAm-*co*-AAc monomer solutions.

Figure 3.6: Steady-state ESA for (a) neutralized Laponite®-doped poly(AAm-*co*-AAc) hydrogels and (b) their neutralized Laponite®-doped AAm-*co*-AAc monomer-solution counterparts: $c_{Lap.} \approx 1$ wt%, $f = 1$ MHz. Colors distinguish $f_{AAc} = 0$–1. Error bars are the standard deviation from time-averaging spectra for $t \approx 100$–150 min. Symbols identify sample replicates.

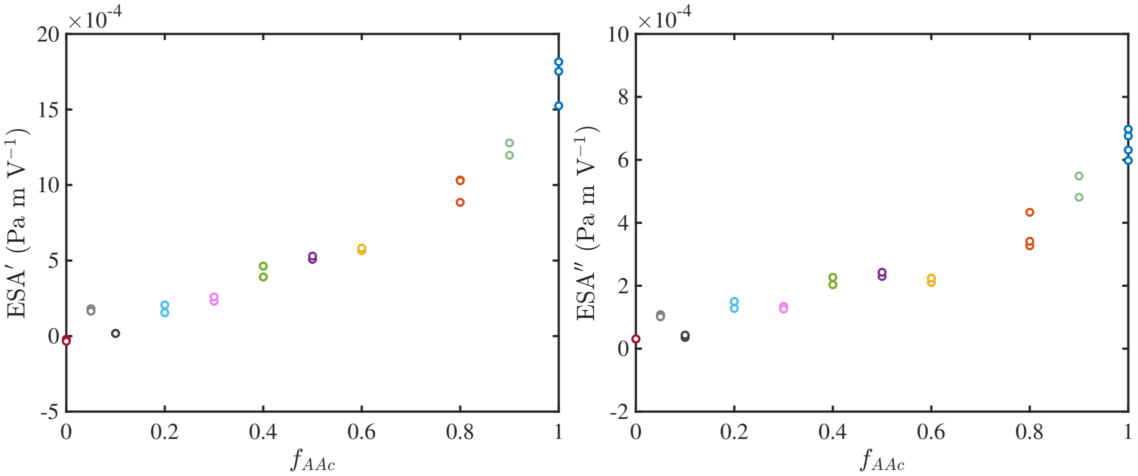

(a) poly(AAm-*co*-AAc) hydrogels.

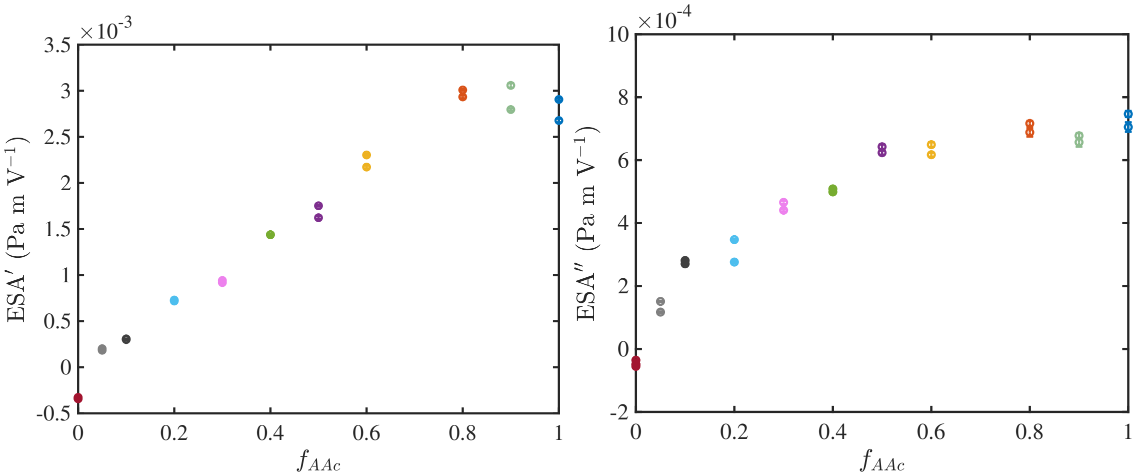

(b) AAm-*co*-AAc monomer solutions.

Figure 3.7: The same as Figure 3.6, but with $f = 14.4$ MHz.

The relatively large (negative) magnitudes of ESA$'$ and ESA$''$ when $f_{AAc} = 0$ are especially notable in the absence of polymerization and cross-linking, but such values are consistent with the ESA for Laponite® in water, for which ESA$' \sim -3 \times 10^{-4}$ Pa m V^{-1}, decreasing to ESA$' \sim -2 \times 10^{-4}$ Pa m V^{-1} in the presence of APS and SMBS (but no AAm or AAc, see the Appendix). While this suggests a weak interaction of AAm monomer with Laponite®, there appears to be a much stronger, significant interaction with AAc$^-$, since any finite concentration of AAc$^-$ negates the otherwise negative ESA$'$. Note that, if AAc$^-$ electrostatically bound to the positive charge on the Laponite® edges, this would shift the net Laponite® charge in the negative direction, similarly shifting ESA$'$, but this is not the case. Nevertheless, such an interaction also transfers mobile AAc$^-$ charge to the Laponite® (with low mobility), thus accentuating the positive contribution to the ESA from Na$^+$ counter-ions. This provides a working hypothesis to be explored when examining hydrogel and monomer-solution conductivities below.

3.4.2 Conductivity

Conductivity time series for Laponite®-doped poly(AAm-*co*-AAc) hydrogels and their monomer-solution counterparts are shown in Figure 3.8. Whereas the monomer solutions in panel (b) tend to establish steady-state conductivities $\lesssim 30$ min , the hydrogel conductivities in panel (a) slowly decrease to steady-state values as gelation progresses over ~ 100 min, particularly for hydrogels with higher charge densities, as measured by f_{AAc}.

The steady-state conductivities for Laponite®-doped poly(AAm-*co*-AAc) hydrogels and their monomer-solution counterparts are compared in Figure 3.9. Although the conductivities vary similarly with respect to f_{AAc}, the values for hydrogels with $f_{AAc} \lesssim 0.15$ are slightly higher than for their monomer-solution counterparts, whereas with $f_{AAc} \gtrsim 0.15$, the conductivities of the hydrogels are notably lower.

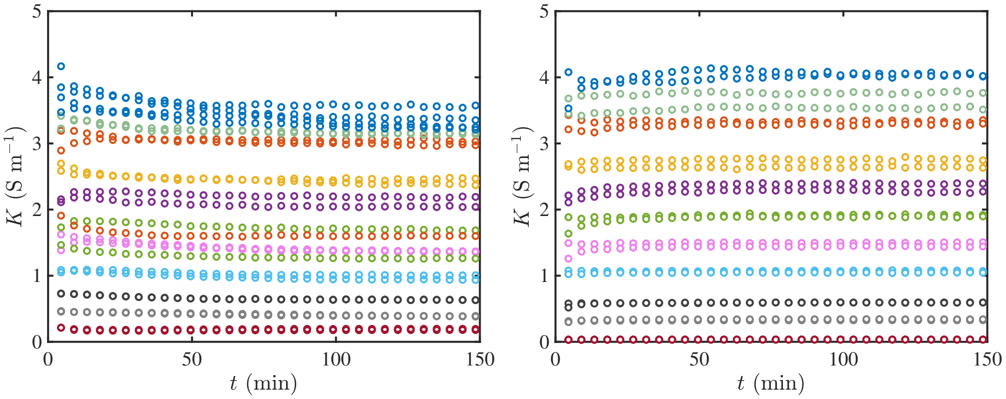

(a) poly(AAm-*co*-AAc) hydrogels. (b) AAm-*co*-AAc monomer solutions.

Figure 3.8: Conductivity time series for neutralized (a) Laponite®-doped poly(AAm-*co*-AAc) hydrogels with $c_{Lap.} \approx 1$ wt% and (b) their monomer-solution counterparts. Colors distinguish $f_{AAc} = 0$–1, as identified in the right panels of Figure 3.7.

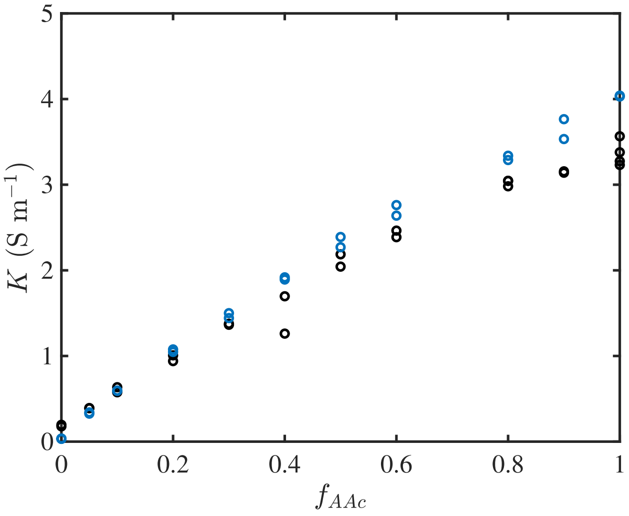

Figure 3.9: Steady-state conductivity for neutralized Laponite®-doped poly(AAm-*co*-AAc) hydrogels (black) and their monomer-solution counterparts (blue) versus the AAc fraction with $c_{Lap.} \approx 1$ wt%.

The higher conductivity of the hydrogels with $f_{AAc} \lesssim 0.15$ reflects the (off-set) contribution of initiator and catalyst, which are absent in the monomer solutions. For hydrogels and monomer solutions with $f_{AAc} \gtrsim 0.15$, the lower conductivity of the hydrogels reflects a hindering of AAc$^-$ mobility by polymerization and cross-linking. It is surprising, perhaps, that the difference is so small. Nevertheless, this is consistent, in part, with Fernandes et al. [2003], who measured the conductivity of 250 kDa PAAc solutions, reporting the molar conductivity (per mer) to be ~ 1 S cm^2 mol^{-1} (at concentrations in the range 1-100 mg l^{-1}), which is more than an order of magnitude lower than the well-known value for Na$^+$ at infinite dilution, ≈ 50.1 S cm^2 mol^{-1}.

Similarly, Adibnia et al. [2020] estimated the molar conductivity of AAc$^-$ monomers in precursor solutions to be $\sim$ 6 S cm^2 mol^{-1} with the hindered molar conductivity of Na$^+$ in poly(AAm-*co*-AAc) hydrogels to be ~ 31.1 S cm^2 mol^{-1}. However, they did not measure the conductivity of AAm-*co*-AAc monomer solutions by systematically varying f_{AAc}. Again, the monomer-solution conductivities in Figure 3.9 suggest that the molar conductivity of AAc$^-$ is very low, assuming, of course, that all AAc monomers are fully dissociated by the neutralization to pH $= 7$.

Table 3.1 compares the conductivities for aqueous solutions with various additives (Laponite®, AAc, APS + SMBS). These highlight the degree to which APS and SMBS increase the conductivity with respect to neat Laponite® in water, as well as an $\approx$ 8% decrease in conductivity that occurs with the addition of 8 wt% AAm to neat Laponite® in water. Note that the sample in table 3.1 containing Laponite® with AAm, APS and SMBS transformed to cloudy, inhomogeneous viscous liquid, whereas the sample without Laponite®, but containing AAm, APS and SMBS, remained a clear, low-viscosity solution, as expected in the absence of TEMED.

Adibnia et al. [2017] noted a decrease in the conductivity of Laponite® XLS solutions with the addition of 5 wt% AAm, decreasing from $K = 0.51$ to 0.43 S m^{-1} (≈ 16%) with Laponite® concentration 2 v% and added electrolytes. They attributed these decrease

Table 3.1: Conductivities K (S m^{-1}) of aqueous Laponite® solutions with $c_{Lap.} = 0.85$ wt%. Mean values ± standard deviation from $n = 2$ replicate samples (exceptions noted).

Lap.	8 wt% AAm	APS+SMBS	K (S m^{-1})
✓	-	-	0.037 ± 0.001
✓	✓	-	0.034 ± 0.001
✓	-	✓	0.24 ± 0.02
✓	✓	✓	0.1724 ± 0.0005 (time average $t = 100$-150 min, $n = 1$)
-	✓	✓	0.163 ± 0.001 (time average $t = 100$-150 min, $n = 1$)

to adsorption of AAm shifting (outward) the NP electrokinetic shear plane. Note that the Laponite® contribution to the conductivity in the polymerized solutions (containing added electrolytes) is $\approx 0.172 - 0.163 = 0.009$ S m^{-1}, which is negligible compared to the conductivity of neat Laponite® in water (≈ 0.037 S m^{-1}) and Laponite® in water with AAm (≈ 0.034 S m^{-1}). Moreover the conductivity of these polymerized samples (≈ 0.172 and 0.163 S m^{-1}) are $\approx 30\%$ lower than for APS and SMBS (with Laponite®) in water (0.24 S m^{-1}). Overall, these data suggest that AAm polymerization, and its role in hindering the mobility of APS and SMBS, is the most significant factor at play.

Figure 3.10 shows the hydrogels conductivities after removing the background contribution of catalyst and initiator (APS and SMBS), as undertaken by Adibnia et al. [2020]. Here, this also removes a weak contribution to the conductivity from Laponite® NPs and their counter-ions. What remains may be interpreted on the basis of the ionic conductivity model of Adibnia et al. [2020] for neutralized poly(AAm-*co*-AAc) hydrogels:

$$\Delta K = K - K(f_{AAc} = 0) = \frac{e^2 c_{AAc}}{6\pi\eta} \frac{\chi_{Na}}{a_{Na}} \left[1 + \frac{(\chi^*_{Na}/\chi_{Na})}{(a_{AAm}/a_{Na})} f_{AAc} \ln(1/f_{AAc}) \right]. \tag{3.17}$$

Fitting this to the data in Figure 3.10 furnishes

$$\Delta K \approx 3.17 f_{AAc}[1 + 0.51 f_{AAc} \ln(1/f_{AAc})], \tag{3.18}$$

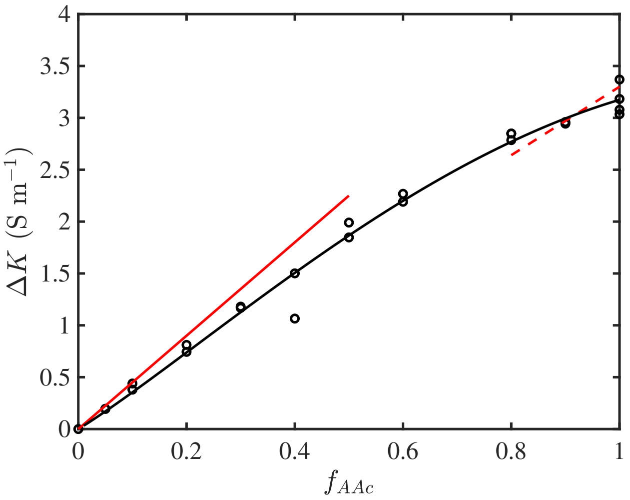

Figure 3.10: Steady-state conductivity for the neutralized Laponite®-doped poly(AAm-*co*-AAc) hydrogels in Figure 3.9, relative to the background value $K(f_{AAc} = 0)$, which includes the contributions of ions that are not AAc$^-$ counter-ions (Na$^+$), i.e., $\Delta K = K - K(f_{AAc} = 0)$. Solid blue line is Eqn. (3.18). Red lines are from Adibnia et al. [2020] for hydrogels with $c_{Lap.} \approx 0$ for $f_{AAc} \to 0$ (solid) and $f_{AAc} \to 1$ (dashed).

which is shown as the black solid line in Figure 3.10. For the same hydrogels without Laponite® NPs, Adibnia et al. [2020] reported

$$\Delta K \approx 4.5 f_{AAc} \text{ for } f_{AAc} \lesssim 0.5 \tag{3.19}$$

and

$$\Delta K \approx 3.3 f_{AAc} \text{ for } f_{AAc} \to 1, \tag{3.20}$$

which are shown as the red lines in Figure 3.10. Thus, when $f_{AAc} \lesssim 0.5$, Laponite®-doping appears to decrease the effective mobility (or effective concentration) of Na$^+$ counter-ions in the poly(AAm-*co*-AAc) network by a factor $\approx 3.2/4.5 \approx 0.7$.

Note that the ratio of the dimensionless pre-factors of the log terms from ESA′ and ΔK [Eqns. (3.15) and (3.18)] is

$$\Delta m_{AAm}/\Delta m_{Na} \approx 0.30/0.51 \approx 0.59.$$

Adibnia et al. [2020] approximated the relative mass of a Na$^+$ ion using the partial-molar volume (-5.4 ml mol^{-1}) and density of water $\rho_w \approx 0.997$ g cm^{-3}, giving $\Delta m_{Na} \approx M_{Na} - \rho_w v_{Na} \approx 28$ g mol^{-1}. The foregoing ratio then gives

$$\Delta m_{AAm} \approx 16 \text{ g mol}^{-1},$$

so with $\Delta m_{AAm} = M_{AAm} - \rho_w v_{AAm}$, the partial molar volume of AAm in solution is estimated (by means of ESA and conductivity here) to be

$$v_{AAm} \approx 55 \text{ cm}^3 \text{ mol}^{-1},$$

which is only about 12% smaller than the partial molar volume of pure AAm, $M_{AAm}/\rho_{AAm} \approx 71/1.13 \approx 63$ cm^3 mol^{-1}. While not intended to furnish a precise measure of the partial molar volume here, the comparison lends support to the foregoing theoretical interpretations of how ESA$'$ and K vary with f_{AAc}.

3.4.3 Rheology

Storage modulus time series for Laponite®-doped hydrogels and their steady-state values are plotted in Figure 3.11. Most samples reach steady-state after ≈ 3 h, somewhat more slowly than the conductivity, but comparable to the ESA. Note that the steady-state storage moduli G'_∞ are from fits of the modified Hill equation [Calvet et al., 2004] to the time series:

$$G'(t) = \frac{G'_\infty t^\alpha}{t^\alpha + \theta^\alpha}, \tag{3.21}$$

where the gelation half-time θ is the time (s) at which $G(\theta) = G'_\infty/2$, and the exponent α furnishes a slope (Pa s^{-1})

$$P = \frac{\alpha G'_\infty}{4\theta}, \tag{3.22}$$

which may be used to quantify the gelation rate.

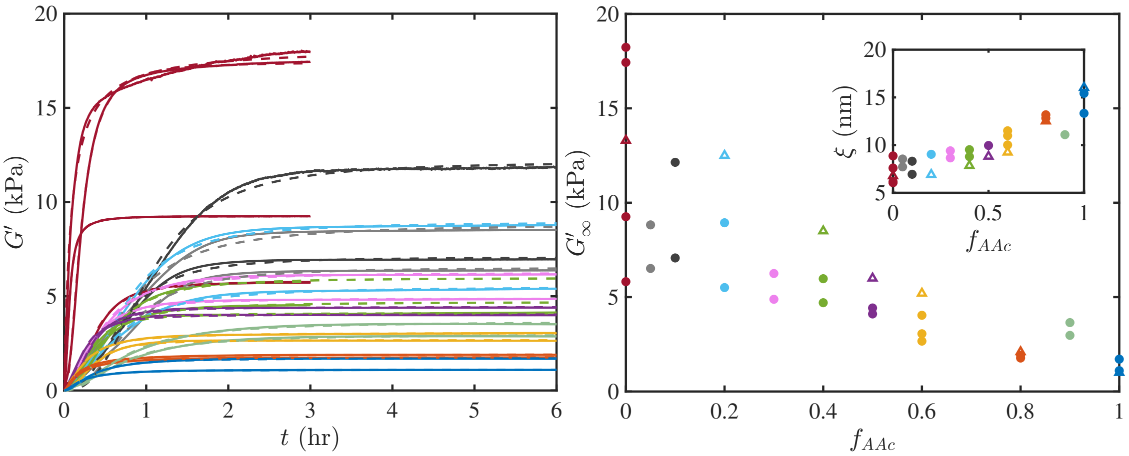

(a) (b)

Figure 3.11: Storage moduli of neutralized Laponite®-doped poly(AAm-*co*-AAc) hydrogels with $c_{Lap.} \approx 1$ (circles, this study) and 0 wt% (triangles, from Adibnia et al. [2020]) and $c_{Lap.} \approx 1$ wt%. (a) Time series data (solid) with fits of Eqn. (3.21) (dashed) for various f_{AAc} [colors identify $f_{AAc} = 0$–1 in panel (b)], and (b) steady-state moduli plotted versus f_{AAc}.

The steady-state storage moduli of Laponite®-doped poly(AAm-*co*-AAc) hydrogels (circles) are comparable to, but consistently lower than, their counterparts without Laponite® NPs (Adibnia et al. [2020], triangles). Thus, similarly to Adibnia et al. [2020], the hydrogel stiffness *decreases* with increasing AAc$^-$ charge, corresponding to an increase in the rheological mesh size

$$\xi = \left(\frac{k_B T}{G'_\infty}\right)^{1/3}, \tag{3.23}$$

where $k_B T$ is the thermal energy (inset of Figure 3.11). Perhaps more surprising is that Laponite® *decreases* the stiffness of the parent hydrogel, suggesting that Laponite® actually modifies the polymerization and cross-linking.

Although sample-to-sample variations tend to increase with decreasing hydrogel charge, some values of G'_∞ for poly(AAm-*co*-AAc) containing Laponite® with $f_{AAc} = 0$ are $\approx$ 5 kPa greater than G'_∞ of their hydrogel counterparts without Laponite®. Such an enhancement of the stiffness is qualitatively consistent with expectations from Zhu et al. [2006], Haraguchi et al. [2007] and Okay and Oppermann [2007], amoung others, which highlight Laponite® NPs as increasing the stiffness of n-isopropylacrylamide and acrylamide-based hydrogels.

Zhu et al. [2006] reported tensile strength, elongation, tensile modulus and swelling ratio for of a series of Laponite® XLS-doped PAAm hydrogels (in situ polymerized without cross-linker). Whereas their PAAm reference hydrogel (10 wt% polymer, cross-linked with 0.1 wt% NMBA) had tensile strength and elongation at break 13.7 kPa and 34.2%, the same PAAm-containing solution (i.e., without chemical cross-linker) doped with 5 wt% Laponite® attained values 107 kPa and 2829%, respectively, albeit with a significantly lower tensile modulus (3.78 versus 40 kPa).

Okay and Oppermann [2007] increased the concentration of Laponite® RDS (bearing only negative charge) concentration from 0.2 to 7 wt%, increasing G' of 5 wt% AAm (NMBA cross-linker to AAm monomer ratio $1/80$) hydrogels by ≈ 6.4 kPa. Aalaie and Youssefi [2011] varied the concentration of Laponite® XLS (bearing only negative charge) from 0 to ≈ 0.4 wt%, increasing G' for hydrogels cross-linked by 0.5 wt% partially hydrolyzed PAAm (chromium triacetate cross-linker to monomer ratio $1/10$) from ≈ 3 to 13 Pa.

Without cross-linker, Adibnia et al. [2017] reported an increase in the storage modulus of a 5 wt% PAAm solution by more than three orders of magnitude with 2 v% Laponite® XLS, transforming the viscoelastic fluid to a viscoelastic solid.

For our AAc containing hydrogels, a *decrease* in G'_∞ with Laponite®-doping when $f_{AAc} > 0$ is contrary to the forgoing expectations gleaned from other PAAm-based hydrogels/solutions. This may be attributed to the high degree of AAc neutralization for our samples (pH ≈ 7). For example, Shen et al. [2014] identified optimal viscosity and stiffness (for nano-composites with 1.5 wt% Laponite® and 20 wt% AAm) when pH ≈ 3.64 with a notable decrease when increasing the pH to 4.68.

Completely neutralizing AAc to achieve pH ≈ 7 presumably increases the repulsive electrostatic interaction between AAc$^-$ monomers and the network, due to the repulsions between the increasing carboxylate ions in the system as the degree of AAc neutralization increases. However, this hypothesis should be further investigated. Based on the accompanying decrease in cross-linking efficiency, the increase of the repulsive interaction promotes the formation of network defects [Du and Hill, 2019]. The decrease in stiffness with Laponite® NPs also suggests that association of uncharged AAm with Laponite® (as identified above from conductivity measurements) may increase the effective value of f_{AAc}, further decreasing the cross-linking efficiency. Based on these considerations, we might expect Laponite NPs to enhance the stiffness of our poly(AAc-*co*-AAm) hydrogels as $f_{AAc} \rightarrow 0$. However, drawing such a conclusion at this stage requires further study to address the relatively large sample-to-sample variations in Figure 3.11 when $f_{AAc} = 0$.

The linear viscoelastic time series of Laponite®-doped poly(AAc-*co*-AAm) hydrogels furnish loss moduli $G''_{\infty} < 0.25$ kPa (available in the Appendix), which are significantly lower than G'_{∞}, thus highlighting the almost ideal elastic solid character of these nanocomposites. Note that G''_{∞} for Laponite®-doped poly(AAc-*co*-AAm) hydrogels are notably higher than for their parent hydrogels, which were reported by Adibnia et al. [2020] to have $G''_{\infty} < 0.01$ kPa. Thus, similarly to Laponite®-doped PAAm hydrogels, the physical association of Laponite® NPs with the polymer network enhances mechanical dissipation, which may improve their toughness. Such (non-linear) rheological analysis is beyond the scope of this particular study, but should be considered in future work.

3.4.4 Laponite® dynamic mobility

The dynamic mobility (magnitude and phase angle) spectra of Laponite® NPs in neutralized poly(AAm-*co*-AAc) hydrogels and their monomer-solution counterparts are shown in Figure 3.12. The mobility is calculated from the ESA spectra according to Eqn. (3.1) with $\rho_p = 2.53$ g/mL, $\rho = 0.998$ g/mL, and ϕ according to a prescribed mass fraction of Laponite® NPs (varying with $c_{Lap.}$) with the instrument software treating the NPs as spheres with the same mass as disks with diameter 25 nm, thickness 1 nm.

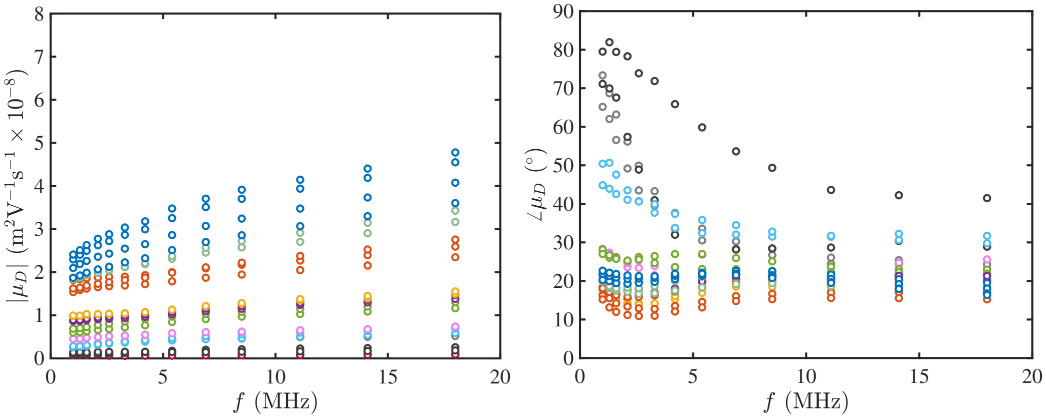

(a) Laponite® in poly(AAm-*co*-AAc) hydrogels.

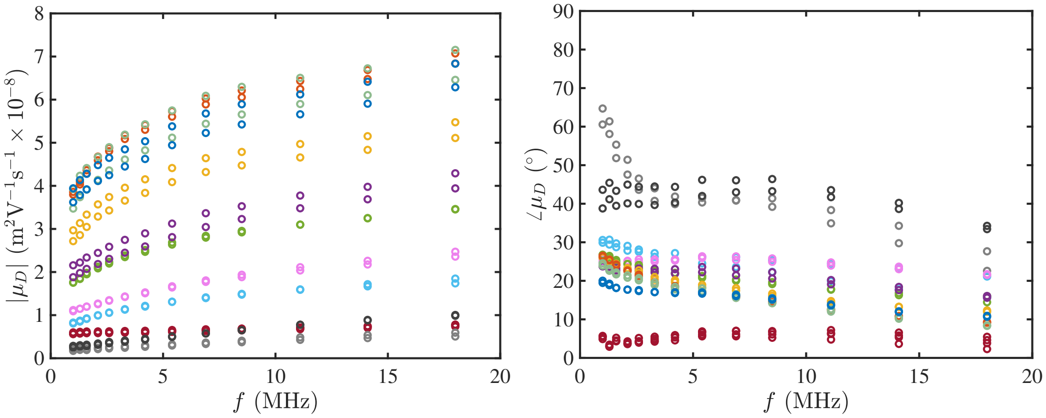

(b) Laponite® in AAm-*co*-AAc monomer solutions.

Figure 3.12: Laponite® NP dynamic mobility spectra in (a) poly(AAm-*co*-AAc) hydrogels and (b) their monomer-solution counterparts with $c_{Lap.} \approx 1$ wt%. Colors distinguish $f_{AAc} = 0$–1, as identified in the right panels of Figure 3.7.

According to Colloidal Dynamics [2000], a negative (positive) mobility argument represents a phase lag (lead), so the apparent electrophoretic velocity of the Laponite® NPs in these hydrogels and monomer solutions exclusively leads the applied electric field. The complex variations in the dynamic mobility with respect to f_{AAc} are different in hydrogels and monomer solutions.

Note that the conversion of ESA to mobility here is far from rigorous because the ESA is dominated by the polymer and monomer signals, not that of the Laponite® NPs, as assumed in the transformation from ESA to dynamic mobility. The dynamic mobility of the Laponite® NPs within the polyelectrolyte hydrogel should be rigorously identified by isolating/separating the NP contribution to the ESA from that of the poly(AAm-*co*-AAc) network. However, this requires systematic variations of the NP and poly(AAm-*co*-AAc) charge density, which is challenging given the low NP concentration and large ESA from the poly(AAm-*co*-AAc) charge. A preliminary study along these lines is presented in the next section.

3.5 Varying Laponite® concentration, fixed AAc fraction

As a preliminary step toward unravelling the effect of Laponite® concentration in poly(AAc-*co*-AAm) hydrogels, the ESA, conductivity, and rheology of samples with $f_{AAc} = 0.5$ are examined in this section, varying $c_{Lap.}$ in the range 0–1 wt%.

Note that repeatability and consistency with published ESA spectra from Adibnia et al. [2020] were established using their batch of AAc (unknown lot #) on poly(AAm-*co*-AAc) hydrogel samples with $f_{AAc} = 0$, 0.1 and 0.3, following the same sample preparation and instrument operation procedures. However, the samples in this section were synthesized from another batch of AAc (lot # MKCM0786), which unexpectedly produced notably different ESA spectra and other properties.

Steady-state ESA data (and their dynamic mobility counterparts) in Figure 3.13 reveal a weak, non-monotonic dependence on Laponite® concentration in panel (c), suggesting that Laponite® in these hydrogels does not significantly modify the hydrogel properties. This may reflect strong electrostatic repulsion between the Laponite® faces and the highly charged polymer network.

Conductivity data in Figure 3.14 also reveal a weak, non-monotonic dependence on Laponite® concentration, as to be expected from the very low concentrations of Laponite® counterions present. Additional ESA, conductivity, and mobility of Laponite® solutions, with and without background ions (APS and SMBS) can be found in the Appendix. Comparing these data with those in Figure 3.8 (from samples synthesized from a different lot/batch of AAc) reveals comparable conductivities.

Similar conclusions may be drawn from the storage modulus in Figure 3.15. What is interesting, perhaps, is that variations with respect to replicate samples tend to be small compared to variations with respect to Laponite® concentration. This suggests a complex systematic variation with respect to Laponite® concentration, but such a relationship seems unlikely, thus motivating further investigation in future studies.

According to Liu et al. [2020] and Shen et al. [2014], the stiffness of PAAm and PAAc hydrogels increases with Laponite® concentration, which these authors varied in the ranges 4.5–15 wt% and 1–2 wt%, respectively. However, as shown in Figure 3.15 (right), only one of 10 Laponite®-doped hydrogels produced a nano-composite with a higher storage modulus than its parent hydrogel. Thus, the steady-state storage modulus is generally lower, albeit with large fluctuations.

As already noted, the high degree of neutralization (complete neutralization to pH $\approx$ 7) of our nano-composites likely promotes electrostatic repulsion between Laponite®-NPs and the polyelectrolyte network, making Laponite® NPs much more passive nanoparticulate fillers under these conditions. Note also that each of our samples was prepared by diluting a concentrated Laponite® stock solution, whereas Shen et al. [2014]

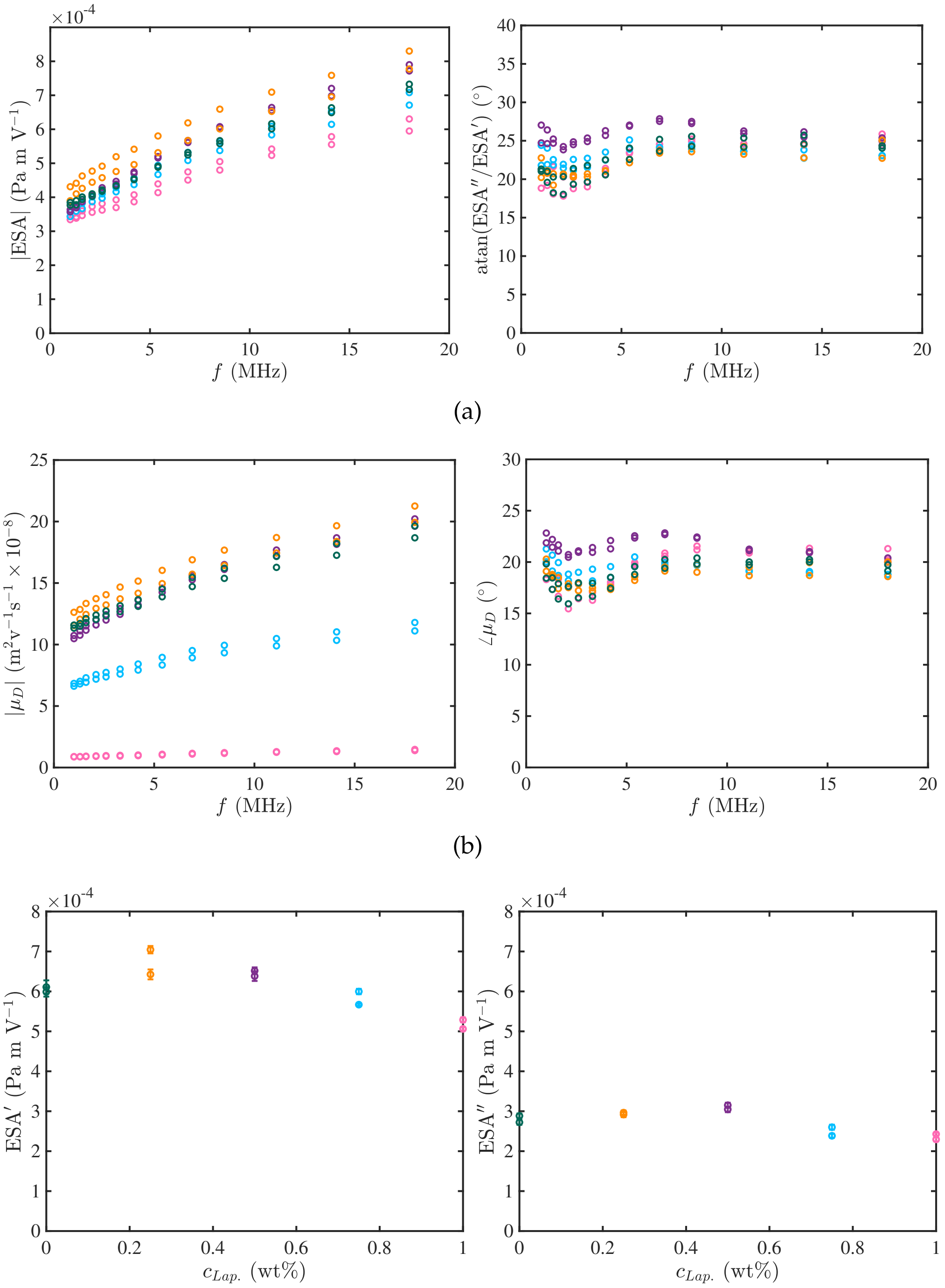

(a)

(b)

(c)

Figure 3.13: ESA of neutralized Laponite®-doped poly(AAm-*co*-AAc) hydrogels with $f_{AAc} = 0.5$. (a) Steady-state ESA magnitude (left) and phase angle (right) spectra. (b) Dynamic mobility spectra from the ESA spectra in (a). (c) Steady-state ESA′ (left) and ESA″ (right) at $f = 14.4$ MHz. Colors distinguish $c_{Lap.}$, as shown in (c).

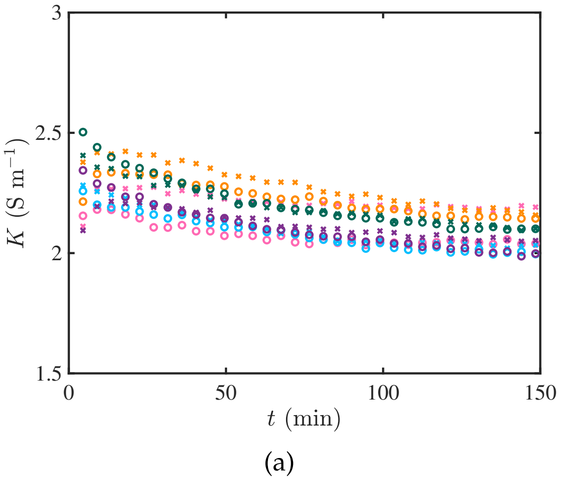

Figure 3.14: Conductivity of neutralized Laponite®-doped poly(AAm-co-AAc) hydrogels with $f_{AAc} = 0.5$. (a) Time series. (b) Steady-state conductivity. Error bars are the standard deviation from time-averaging over $t = 130$–150 min. Colors distinguish $c_{Lap.}$, identified in (b).

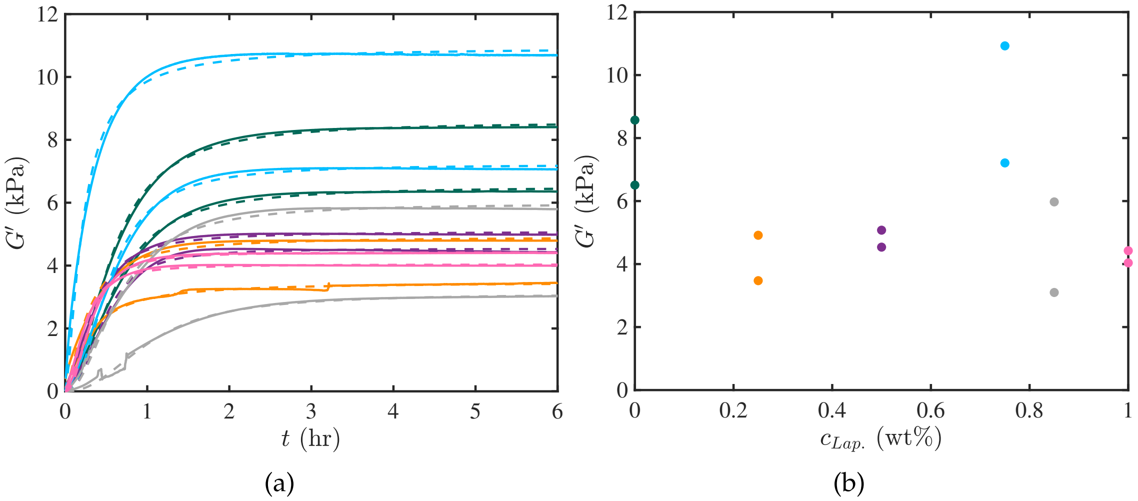

Figure 3.15: (a) Storage-modulus time series (solid) with fits of Eqn. (3.21) (dashed). (b) Steady-state storage modulus of neutralized Laponite®-doped poly(AAm-*co*-AAc) hydrogels with $f_{AAc} = 0.5$. Colors distinguish $c_{Lap.}$, identified in (b).

dispersed Laponite® powder with water containing hydrogel precursors, mixing each solution for > 4 h prior to gelation. These considerations likely impact the way in which Laponite® XLG interacts with itself, impacting, for example, exfoliation [Sheikhi et al., 2018] and NP clustering. Again, such details are beyond the scope of the present study, but need to be carefully considered in future work.

3.6 Conclusions

Laponite® NPs were added to the poly(AAm-*co*-AAc) hydrogels of Adibnia et al. [2020]. After neutralizing the Laponite®-doped pre-gel solutions, the solutions gelled by free-radical polymerization and cross-linking. AAm-*co*-AAc monomer solutions were also prepared to help understand the effects of polymerization and cross-linking on the nanocomposite ESA, electrical conductivity, viscoelastic rheology, and dynamic mobility.

All components of the complex-valued ESA spectra increased with the AAc fraction f_{AAc}, attributed mainly to the accompanying Na^+ counterion concentration. A mechanistic model extending the model of Adibnia et al. [2020] for poly(AAm-*co*-AAc) hydrogels was fitted to ESA′ for Laponite®-doped poly(AAm-*co*-AAc) networks at $f = 1$ MHz. A small, additive constant in the formula capturing how ESA′ depends on f_{AAc} captures the Laponite® NP and counterion (Na^+ and OH^-) contributions to the total ESA.

Noteworthy is that AAm-*co*-AAc monomer solutions (without initiator, catalyst, or cross-linker) registered a higher ESA than their polymerized and cross-linked poly(AAc-*co*-AAm) hydrogel counterparts. This is consistent with the model of Adibnia et al. [2020], which identifies a small, negative ESA′ for weakly charged poly(AAc-*co*-AAm) hydrogels. More importantly, the experiments conducted in this study confirm that the negatively signed ESA′ vanishes in the absence of cross-linking.

Further testing of the model was undertaken by examining the conductivities of the hydrogels, subtracting a constant background contribution from the Laponite®, counter-ions, and precursor ions. The resulting variation of the poly(AAc-*co*-AAm) network conductivity with respect to f_{AAc} was well described by the model of Adibnia et al. [2020] over the full range of $f_{AAc} = 0$–1. Noteworthy is that the ratio of dimensionless prefactors of the log terms in the ESA′ and conductivity formulas furnished the partial molar volume of AAm (in the polymerized state). This which was found to be within $\approx 10\%$ of the value for pure AAm (as calculated by it molecular weight and bulk density).

The storage modulus of Laponite®-doped poly(AAm-*co*-AAc) hydrogels decreased with increasing f_{AAc}, similarly to the parent hydrogels of Adibnia et al. [2020], albeit registering consistently lower values with Laponite®-doping. For samples with $f_{AAc} > 0$, G' decreased from $\approx$ 7 to 1 kPa, whereas the storage modulus of the parent hydrogels decreased from ≈ 12 to 1 kPa over the same range $0 < f_{AAc} \leq 1$.

Contrary to many previous studies of how Laponite® tends to increase stiffness, the stiffness of the poly(AAm-*co*-AAc) hydrogels in this study were notably indifferent to Laponite®-doping. This seems to reflect a repulsive electrostatic interaction between the NPs and poly(AAm-*co*-AAc) network, transforming the more customary attraction between protonated carboxyl groups and Laponite®[Shen et al., 2014] to electrostatic repulsion.

Because Laponite®-doping slightly decreases nano-composite stiffness, the NPs are suggested to also modify the polymerization and cross-linking, decreasing the effective cross-linking density, increasing network defects, increasing dissipation, etc. These inferences are consistent with those drawn from ESA. An electrostatic repulsion between Laponite® and the poly(AAm-*co*-AAc) networks would seem to promote Laponite® diffusion and transport in these nanocomposites, an hypothesis that needs to be tested in future experiments, perhaps aided by dynamic light-scattering diagnostics.

Bibliography

J. Aalaie and M. Youssefi. Study on the dynamic rheometry and swelling properties of the polyacrylamide/laponite nanocomposite hydrogels in electrolyte media. *J. Macromol. Sci. Part B Phys.*, 51, 01 2011.

V. Adibnia and R. J. Hill. Electroacoustic Spectroscopy of Nanoparticle-Doped Hydrogels. *Macromolecules*, 47(22):8064–8071, 2014.

V. Adibnia, K. W. Cho, and R. J. Hill. Nanoparticle Coupling to Hydrogel Networks: New Insights from Electroacoustic Spectroscopy. *Macromolecules*, 50(10):4030–4038, May 2017.

V. Adibnia, G. Afuwape, and R. J. Hill. Electrokinetic sonic amplitude of polyelectrolyte solutions and networks. *Macromolecules*, 53:7460–7468, 2020.

F. Becerra-Bracamontes, J. C. Sánchez-Díaz, A. González-Álvarez, P. Ortega-Gudiño, E. Michel-Valdivia, and A. Martínez-Ruvalcaba. Design of a drug delivery system based on poly(acrylamide-co-acrylic acid)/chitosan nanostructured hydrogels. *J. Appl. Polym. Sci.*, 106(6):3939–3944, 2007.

T. B. Becher, C. B. Braga, D. L. Bertuzzi, M. D. Ramos, A. Hassan, F. N. Crespilho, and C. Ornelas. The structure–property relationship in LAPONITE® materials: from Wigner glasses to strong self-healing hydrogels formed by non-covalent interactions. *Soft Matter*, 15(6):1278–1289, 2019.

P. S. Bhosale, J. Chun, and J. C. Berg. Electroacoustics of particles dispersed in polymer gel. *Langmuir*, 27(12):7376–7379, 2011.

D. Calvet, J. Y. Wong, and S. Giasson. Rheological monitoring of polyacrylamide gelation importance of cross-link density and temperature. *Macromolecules*, 37(20):7762–7771, 2004.

S. Çavuş, G. Gürdağ, K. Sözgen, and M. A. Gürkaynak. The preparation and characterization of poly(acrylic acid-co-methacrylamide) gel and its use in the non-competitive heavy metal removal. *Polym. Adv. Technol.*, 20(3):165–172, 2009.

Y. Chen, Y. Peng, W. Liu, X. Li, and X. Yan. Effect of amps and clay on the acrylic acid based superabsorbent hydrogels. *Appl. Mech. Mater.*, 427-429:364–367, 09 2013.

Colloidal Dynamics. How do the zetaprobe and acoustosizer ii measure zeta potential and particle size? Technical report, Colloidal Dynamics, 2000.

H. Z. Cummins. Liquid, glass, gel: The phases of colloidal laponite. *J. Non. Cryst. Solids.*, 353(41):3891–3905, 2007.

S. P. O. Danielsen, H. K. Beech, S. Wang, B. M. El-Zaatari, X. Wang, L. Sapir, T. Ouchi, Z. Wang, P. N. Johnson, Y. Hu, D. J. Lundberg, G. Stoychev, S. L. Craig, J. A. Johnson, J. A. Kalow, B. D. Olsen, and M. Rubinstein. Molecular characterization of polymer networks. *Chem. Rev.*, 121(8):5042–5092, 2021.

C. Du and R. J. Hill. Linear viscoelasticity of weakly cross-linked hydrogels. *J. Rheol.*, 63 (1):109–124, 2019.

A. L. P. Fernandes, R. R. Martins, C. G. da Trindade Neto, M. R. Pereira, and J. L. C. Fonseca. Characterization of polyelectrolyte effect in poly(acrylic acid) solutions. *J. Appl. Polym. Sci.*, 89:191–196, 2003.

K. Haraguchi, H.-J. Li, L. Song, and K. Murata. Tunable optical and swelling/deswelling properties associated with control of the coil-to-globule transition of poly(n-isopropylacrylamide) in polymer-clay nanocomposite gels. *Macromolecules*, 40(19): 6973–6980, 2007.

V. Kurenkov, H.-G. Hartan, and F. Lobanov. Application of polyacrylamide flocculants for water treatment. *Butlerov Commun.*, 3, 01 2002.

P. Li, Siddaramaiah, N. H. Kim, S.-B. Heo, and J.-H. Lee. Novel paam/laponite clay nanocomposite hydrogels with improved cationic dye adsorption behavior. *Composites, Part B*, 39(5):756–763, 2008.

J. Ling, N. Li, X. Yang, J. Ma, J. Du, D. Wang, Y. Tan, F. Yue, and S. Xu. Strengthening mechanism of poly(acrylamide)/graphene oxide/laponite dual nanocomposite hydrogels. *J. Appl. Polym. Sci.*, 134(24), 2017.

X. Liu, X. Niu, Z. Fu, L. Liu, S. Bai, J. Wang, L. Li, Y. Wang, and X. Guo. A facile approach to obtain highly tough and stretchable laponites-based nanocomposite hydrogels. *Soft Matter*, 16:8394–8399, 2020.

S. Merino, C. Martín, K. Kostarelos, M. Prato, and E. Vázquez. Nanocomposite Hydrogels: 3D Polymer–Nanoparticle Synergies for On-Demand Drug Delivery. *ACS Nano.*, 9(5):4686–4697, 2015.

S. Ngema, A. Basson, and T. Maliehe. Synthesis, characterization and application of polyacrylamide grafted bioflocculant. *Phys. Chem. Earth. A/B/C*, 115:102821, 2020.

R. O'Brien, D. Cannon, and W. Rowlands. Electroacoustic determination of particle size and zeta potential. *J. Colloid Interface Sci.*, 173(2):406–418, 1995.

R. O'Brien, A. Jones, and W. Rowlands. A new formula for the dynamic mobility in a concentrated colloid. *Colloids Surf A*, 218(1):89–101, 2003.

O. Okay and W. Oppermann. Polyacrylamide-clay nanocomposite hydrogels: Rheological and light scattering characterization. *Macromolecules*, 40:3378–3387, 2007.

K. A. B. Pereira, K. L. N. P. Aguiar, P. F. Oliveira, B. M. Vicente, L. G. Pedroni, and C. R. E. Mansur. Synthesis of hydrogel nanocomposites based on partially hydrolyzed polyacrylamide, polyethyleneimine, and modified clay. *ACS Omega*, 5(10):4759–4769, 2020.

M. T. Radoiu, D. I. Martin, I. Calinescu, and H. Iovu. Preparation of polyelectrolytes for wastewater treatment. *J. Hazard. Mater.*, 106(1):27–37, 2004.

Rockwood Additives Ltd. Laponite: performance additives, 2013.

F. Sabbagh and I. I. Muhamad. Acrylamide-based hydrogel drug delivery systems: Release of acyclovir from mgo nanocomposite hydrogel. *J. Taiwan Inst. Chem. Eng.*, 72: 182–193, 2017.

P. Schexnailder and G. Schmidt. Nanocomposite polymer hydrogels. *Colloid Polym. Sci.*, 287:1–11, 2009.

N. Sediiki, D. Aliouche, and I. BOUDHENE. Preparation of nanocomposite hydrogels with nanoclay: characterization, swelling properties and dye adsorption behavior. *Rev. Roum. Chim.*, 65:119–133, 01 2020.

A. Shahin and Y. M. Joshi. Physicochemical effects in aging aqueous laponite suspensions. *Langmuir*, 28(44):15674–15686, 2012.

A. Sheikhi, S. Afewerki, R. Oklu, A. K. Gaharwar, and A. Khademhosseini. Effect of ionic strength on shear-thinning nanoclay–polymer composite hydrogels. *Biomater. Sci.*, 6(8): 2073–2083, 2018.

M. Shen, L. Li, Y. Sun, J. Xu, X. Guo, and R. K. Prud'homme. Rheology and adhesion of poly(acrylic acid)/laponite nanocomposite hydrogels as biocompatible adhesives. *Langmuir*, 30(6):1636–1642, Feb. 2014.

B. Singh, V. Sharma, Rohit, and A. Kumar. Designing moringa gum-sterculia gum-polyacrylamide hydrogel wound dressings for drug delivery applications. *Carbohydr. Polym.*, 2:100062, 2021.

G. Singh, A. Lohani, and S. S. Bhattacharya. Hydrogel as a novel drug delivery system: a review. *J. Fundam. Pharm. Res.*, 2(1):35–48, 2014.

C. Srivastava, P. Rajput, and R. Purwar. Composite wound dressing for drug release. *Fibers Polym.*, 15:1422–1428, 02 2014.

G. Valencia, M. Djabourov, F. Carn, and P. Sobral. Novel insights on swelling and dehydration of laponite. *Colloid Interface Sci. Commun.*, 23:1–5, 2018.

B. Xiong, R. Loss, D. Shields, T. Pawlik, R. Hochreiter, A. Zydney, and M. Kumar. Polyacrylamide degradation and its implications in environmental systems. *npj Clean Water*, 1, 12 2018.

J.-Z. Yi and L.-M. Zhang. Removal of methylene blue dye from aqueous solution by adsorption onto sodium humate/polyacrylamide/clay hybrid hydrogels. *Bioresour. Technol.*, 99(7):2182–2186, 2008.

X. Zhang, S. Zheng, Z. Lin, and J. Zhang. Removal of basic fuchsin dye by adsorption onto polyacrylamide/laponite nanocomposite hydrogels. *Synthesis and Reactivity in Inorganic, Metal-Organic, and Nano-Metal Chemistry*, 42(9):1273–1277, 2012.

Y. Zhang. Preparation of copolymers of acrylic acid and acrylamide for copper (ii) capture from aqueous solutions. Master's thesis, University of Waterloo, 2009.

H. Zhao, M. Liu, Y. Zhang, J. Yin, and R. Pe. Nanocomposite hydrogels for tissue engineering applications. *Nanoscale*, 12:14976–14995, 2020.

M. Zhu, Y. Liu, B. Sun, W. Zhang, X. Liu, H. Yu, Y. Zhang, D. Kuckling, and H.-J. P. Adler. A novel highly resilient nanocomposite hydrogel with low hysteresis and ultrahigh elongation. *Macromol. Rapid Commun.*, 27:1023–1028, 2006.

Chapter 4

Summary and future work

This thesis sought to advance our fundamental understanding of Laponite$^{®}$-doped charged poly(AAm-*co*-AAc) hydrogels and monomer solutions by studying their electroacoustic responses, electrical conductivity, linear rheology, and dynamic mobility. The objectives identified in Chapter 1.2 were pursued, and the outcomes are summarized as follows.

By comparison with Adibnia et al. [2020], who studied neat poly(AAm-*co*-AAc) hydrogels, the effects of Laponite$^{®}$ with $c_{Lap.} \leq 1$ wt% on the ESA of poly(AAm-*co*-AAc) hydrogels were of particular interest. Whereas ESA$'$ and ESA$''$ (and therefore $|\mathrm{M}|$) increased with respect to f_{AAc}, the phase angle decreased, exhibiting significantly larger values than reported by Adibnia et al. [2020] for neat poly(AAm-*co*-AAc) hydrogels. These observations suggest that Laponite$^{®}$ decreases the stiffness of the poly(AAm-*co*-AAc) networks, but increase the dissipation, as tested by studying the linear viscoelasticity.

The mechanistic model of Adibnia et al. [2020] for ESA$'$ of poly(AAm-*co*-AAc) networks could be fit to data for Laponite$^{®}$-doped poly(AAm-*co*-AAc) networks, revealing a smaller dimensionless pre-factor of the log term. Nevertheless, this model was extended to explicitly account for Laponite$^{®}$ and counter-ions, thus introducing an additional constant (ESA$'$ for an uncharged hydrogel with charged NPs and their counter-ions), which was found to be negative. This reflects a net negative, albeit weak, contribution to the

ESA arising from the net negatively charged Laponite® and the positive and negative counter-ions (assumed to be Na^+ and OH^-).

Laponite® did not significantly change hydrogel conductivity K, as expected from the relatively small number of counter-ions. Interestingly, however, polymerization and cross-linking decreased the hydrogel conductivities relative to their AAm-*co*-AAc monomer-solution counterparts. Subtracting a small constant contribution to the conductivity, from (i) Laponite® and its counter-ions and (ii) precursor ionic species, isolated the contributions to the nano-composite conductivities from AAc^- and its Na^+ counter-ions. This relationship was then theoretically interpreted by fitting the ionic conductivity model of Adibnia et al. [2020], furnishing a good fit over the full range of $f_{AAc} = 0$–1.

From the foregoing theoretical interpretations of how ESA′ and K vary with respect to f_{AAc}, the partial molar volume of AAm in solution (as a polymer) could be estimated, furnishing a value that was within $\approx 10\%$ of the partial molar volume of pure AAm (based on its bulk density and molecular weight).

The linear viscoelastic response of Laponite®-doped poly(AAm-*co*-AAc) networks furnished a steady-state storage modulus that decreased with increasing polymer charge density, as measured by f_{AAc} in the range 0–1. While this is qualitatively similar to the neat poly(AAm-*co*-AAc) hydrogels studied by Adibnia et al. [2020], 1 wt% Laponite® in hydrogels with $f_{AAc} > 0$ decreased the stiffness by a statistically significant amount, albeit decreasing with increasing f_{AAc}. For uncharged hydrogels ($f_{AAc} = 0$), the storage modulus varied considerably (in the range ≈ 5–20 kPa) with respect to replicate samples.

Whereas most literature has focussed on enhancements of the mechanical and rheological characteristics of AAm- and AAc-based hydrogels and solutions by Laponite®, the high degree of neutralization to $\mathrm{pH} = 7$ in this study revealed a significantly different NP-polymer interaction, leading to more compliant and dissipative microstructure. This might be interpreted in terms of a transformation from an attraction interaction between Laponite® and protonated carboxyl groups of poly(AAm-*co*-AAc) to a repulsion between

Laponite® and ionized AAc$^-$ moieties in the neutralized poly(AAm-*co*-AAc) network. However, there remains an electrostatic attraction between AAc$^-$ moieties and the positively charged Laponite® edges. These may be negated during the pre-polymerization due to AAc$^-$ monomers electrostatically binding to the Laponite® edges, thus prohibiting "house-of-cards" structures and decreasing the effective concentration of AAc$^-$ available for polymerization. A detailed picture of how this might affect the rheological and mechanical properties is presently unknown, and should be studied in future research, perhaps assisted by light- (and other) scattering methods.

Finally, attempts to systematically vary the Laponite® concentration posed challenges due to large uncontrolled sample-to-sample variations in nano-composite properties, and the relatively low concentrations of Laponite® that could be dispersed in their pre-gel solutions. For example, attempts to separate the Laponite® ESA from the total ESA (to furnish the NP dynamic mobility), were frustrated by a relatively weak contribution of the NPs and the large, uncontrolled sample-to-sample variations in hydrogel rheological properties. Note that these experiments were undertaken with a new batch/lot of AAc, which produced hydrogels with notably different properties than from the batch/lot used in the main body of this work and in the published study of Adibnia et al. [2020]. Reasons for such batch-to-batch variations are presently unknown, and should be explicitly considered in future research.

Bibliography

V. Adibnia, G. Afuwape, and R. J. Hill. Electrokinetic sonic amplitude of polyelectrolyte solutions and networks. *Macromolecules*, 53:7460–7468, 2020.

Appendix A

Supporting experimental data

A.1 Repeatability of ESA and conductivity for poly(AAm-*co*-AAc) hydrogels

Repeatability and consistency with respect to experiments conducted by Adibnia et al. [2020] were tested using poly(AAm-*co*-AAc) hydrogels (without nanoparticles) with $f_{AAc} = 0$, 0.1, and 0.3, following the same sample preparation and instrument operation procedures. Note that these experiments were conducted using the same AAc lot as Adibnia et al. [2020], providing acceptable correspondence, as demonstrated by ESA and conductivity time series shown in Figure A.1.

A.2 ESA, conductivity, and dynamic mobility for Laponite® solutions

Figures A.2 and A.3 show ESA, conductivity and dynamic mobility data for Laponite® solutions with and without the catalyst (APS) and initiator (SMBS). Laponite® size and concentration were prescribed (to compute mobility from ESA) as described in the main text.

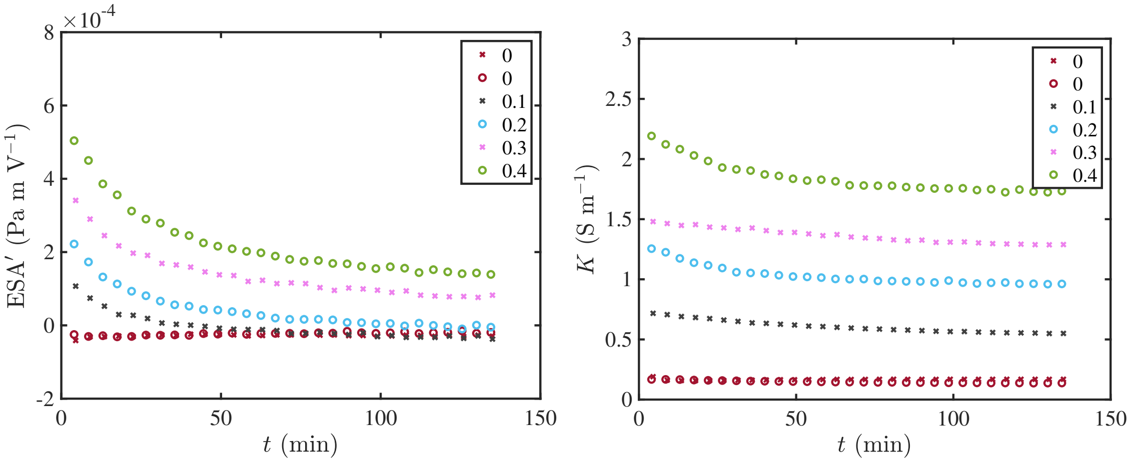

(a)

(b)

Figure A.1: (a) ESA′ ($f = 14.4$ MHz) and (b) conductivity K time series of neutralized poly(AAm-*co*-AAc) hydrogels (without nanoparticles) with $f_{AAc} = 0$, 0.1, 0.2, 0.3, 0.4 (colors and symbols in the legend). Circles are from Adibnia et al. [2020], and crosses are tests of repeatability.

A.3 Impact of gas bubbles on ESA and conductivity of poly(AAm-*co*-AAc) hydrogels

Figures A.5 and A.6 demonstrate a negligible impacts of vigorously shaking pre-gel solutions (to increase the small bubble volume fraction) prior to injection into the ESA sample holder.

A.4 Linear viscoelasticity of Laponite®-doped poly(AAm-*co*-AAc) hydrogels

Figure A.7 shows steady-state dynamic moduli for Laponite®-doped poly(AAm-*co*-AAc) hydrogels, varying (a) the AAc monomer fraction f_{AAc} with fixed Laponite® concentration and (b) the Laponite® concentration at fixed AAc monomer fraction f_{AAc}.

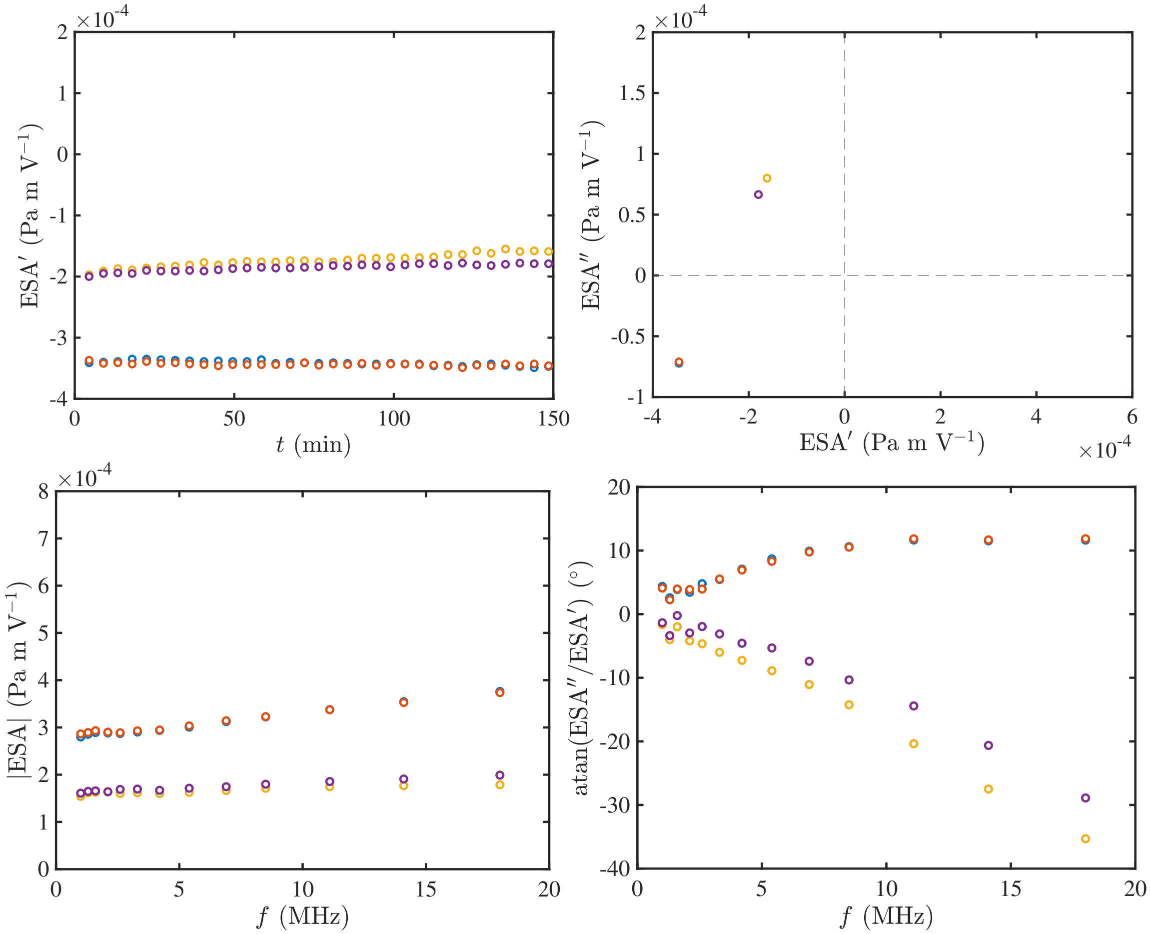

Figure A.2: ESA of Laponite® solutions ($c_{Lap.} \approx 1$ wt%) with (yellow and violet) and without catalyst (APS) and initiator (SMBS) (blue and red). Argand diagram of full spectra (time-averaging over $t = 135$–150 min).

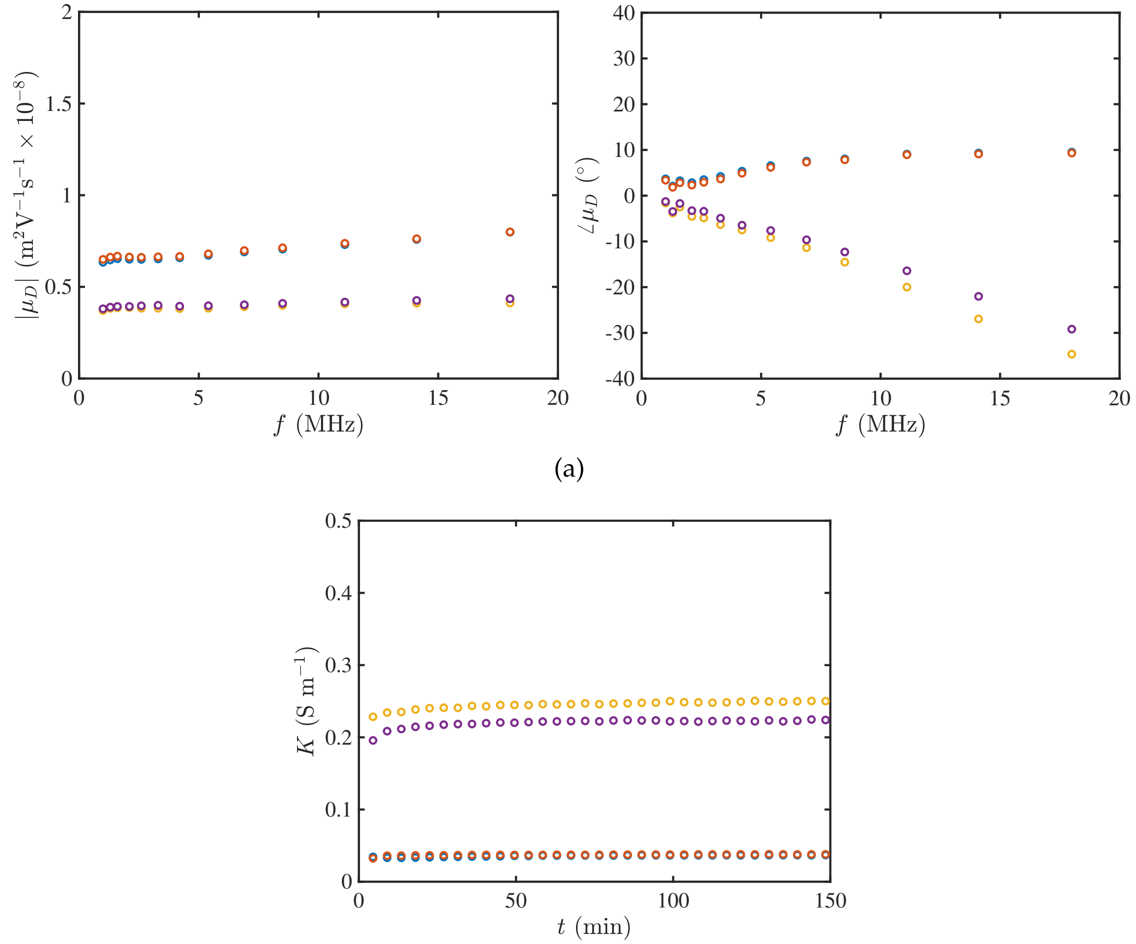

(a)

(b)

Figure A.3: Dynamic mobility μ_D (a, magnitude and phase angle spectra) and conductivity K time series (b) of the Laponite® solutions in Figure A.2.

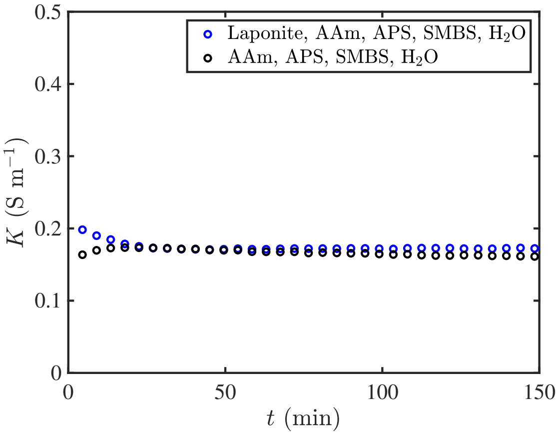

Figure A.4: Conductivity time series for two of the conductivity measurements reported in table 3.1 of the main text. The Laponite®-containing solution (blue) forms a viscous, cloudy solution, whereas the other is colorless, transparent.

Bibliography

V. Adibnia, G. Afuwape, and R. J. Hill. Electrokinetic sonic amplitude of polyelectrolyte solutions and networks. *Macromolecules*, 53:7460–7468, 2020.

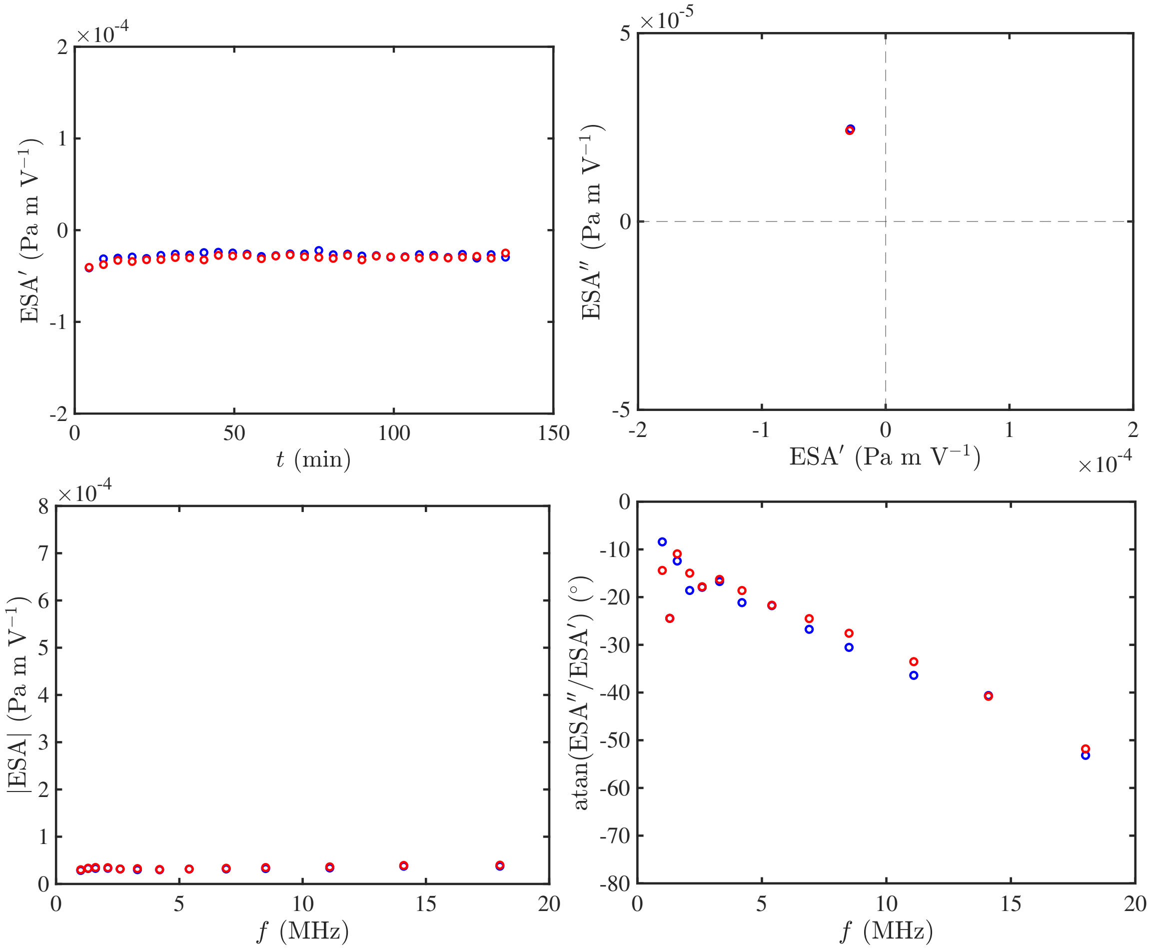

Figure A.5: ESA of poly(AAm-*co*-AAc) hydrogels ($f_{AAc} = 0$) with (red) and without (blue) vigorous shaking of the pre-gel solution prior to injection into the ESA sample holder. Argand diagram of full spectra (time-averaging over $t = 135$–150 min).

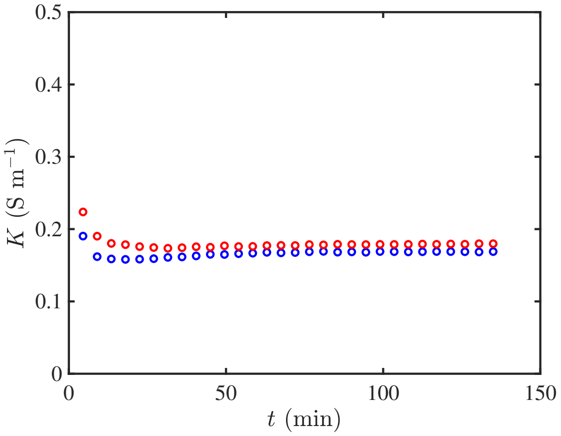

Figure A.6: Conductivity of the poly(AAm-*co*-AAc) hydrogels in Figure A.5.

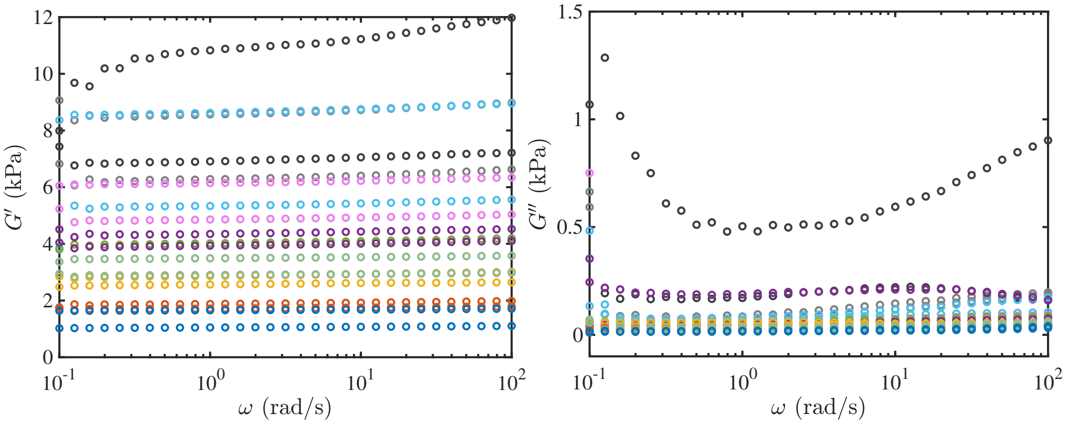

(a) $c_{Lap.} = 1$ wt%, $f_{AAc} = 0$–1.

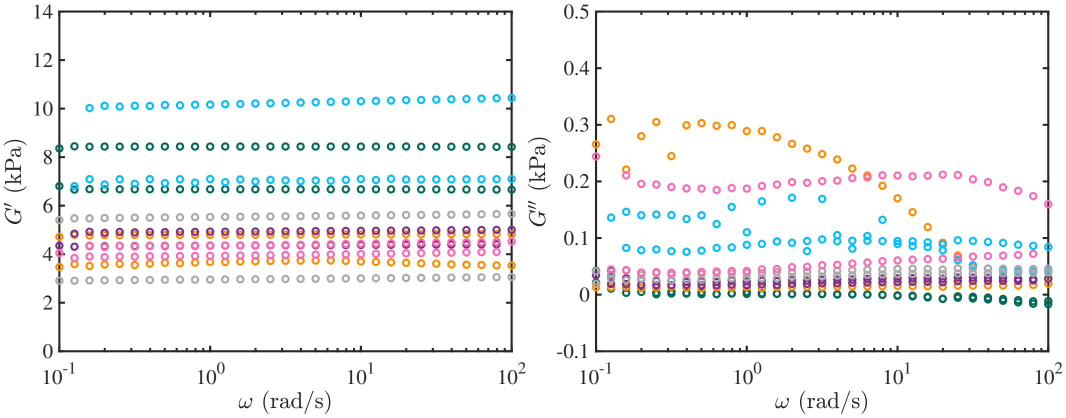

(b) $c_{Lap.} = 0$–1 wt%, $f_{AAc} = 0.5$.

Figure A.7: Steady-state dynamic moduli spectra ($\gamma = 0.02$) of Laponite®-doped poly(AAm-*co*-AAc) hydrogels. (a) $c_{Lap.} = 1$ wt% and $f_{AAc} = 0$–1 (identified in figure 3.11 of the main text). (b) $c_{Lap.} = 0$–1 wt% (identified in figure 3.15 of the main text) and $f_{AAc} = 0.5$.